

On the time evolution of giant radio galaxies

J. Machalski,^{1*}K.T. Chyży,¹ M. Jamrozy²

¹Astronomical Observatory, Jagellonian University, ul. Orła 171, PL-30244 Cracow, Poland

²Radioastronomisches Institut der Universität Bonn, Auf dem Hügel 71, D-53121 Bonn, Germany

November 13, 2018

Abstract

A time evolution of *giant* lobe-dominated radio galaxies (with projected linear size $D > 1$ Mpc for $H_0=50$ km s⁻¹Mpc⁻¹ and $q_0=0.5$) is analysed on the basis of dynamical evolution of the entire FR II-type population. Two basic physical parameters, namely the jet power Q_0 and central density of the galaxy nucleus ρ_0 are derived for a sample of *giants* with synchrotron ages reliably determined, and compared with the relevant parameters in a comparison sample of normal-size sources consisting of 3C, B2, and other sources. Having apparent luminosity (power) P and linear size D of each sample source, Q_0 and ρ_0 are fitted using the dynamical model of Kaiser et al. (1997) but modified by allowing an evolution of the cocoon axial ratio with time as suggested by Blundell et al. (1999). In a result, we found that: (i) there is not a unique factor governing the source size; *giants* are old sources with high enough jet power evolved in a relatively low-density environment. The size is dependent, in order of decreasing partial correlation coefficients, on age; then on Q_0 ; next on ρ_0 , (ii) a number of the sample sources, having similar Q_0 and ρ_0 but different ages and axial ratios (called a ‘clan’), fit very well the evolutionary luminosity–size (P – D) and energy density–total energy (u_{eq} – E_{tot}) tracks derived from the model for a ‘fiducial’ source with Q_0 and ρ_0 equal to the means of relevant values obtained for the ‘clan’ members. Therefore, these sources can be considered as ‘the same’ source observed at different epochs of its lifetime, and hence very useful for an ob-

servational constraint of evolutionary models of the source dynamics, (iii) in some cases a slow acceleration of the average expansion speed of the cocoon along the jet axis seems to be present, and (iv) apparent increase of the lowest internal pressure value, observed within the largest sources’ cocoon, with redshift is obscured by the intrinsic dependence of their age on redshift, which hinders making definite conclusions about a cosmological evolution of intergalactic medium (IGM) pressure.

1 Introduction

Extragalactic radio sources, powered by twin jets resulting from nuclear energy processes in the Active Galactic Nucleus (AGN), exhibit a very large span of their linear size. The sizes of these powerful sources range from less than 10² pc (GPS: gigahertz-peaked spectrum), through 10²–10⁴ pc (CSS: compact steep spectrum), 10⁴–10⁶ pc (normal-size sources), up to greater than 10⁶ pc \equiv 1 Mpc (‘giant’ radio sources). One of the key problems of the evolution of extragalactic sources is whether and how different size sources are related. Is there a single evolutionary scheme governing the size evolution of radio sources, or do small and large sources evolve in a different way?

From many years ‘giant’¹ radio sources are of a special interest for several reasons. Their very large angular sizes give excellent opportunity for the study of

¹hereafter we use *giant* or *giants* instead of giant radio source(s)

*Email: machalsk@oa.uj.edu.pl

source physics. They are also very useful to study the density and evolution of the intergalactic and intra-cluster environment (cf. Subrahmanyan & Saripalli 1993; Mack et al. 1998), as well as to verify the unification scheme for powerful radio sources (Barthel 1989; Urry & Padovani 1995). Finally, they can be used to constrain dynamical models of the source time evolution (e.g. Kaiser & Alexander 1999). The general questions are: do the largest radio sources reach their extremal *giant* sizes due to (i) exceptional physical conditions in the intergalactic medium, (ii) extraordinary intrinsic properties of the AGN, or simply (iii) because they are extremely old?

To answer these questions, in a number of papers the attempts were undertaken to recognize eventual other properties but size which may differentiate *giants* from normal-size sources. The *giant*-source morphologies, energy density in the lobes and interaction with the intergalactic medium were studied by Subrahmanyan et al. (1996), who suggested that *giant* radio galaxies may be located in the lowest density regions, and ‘may attained their large size as a result of restarting of their central engines in multiple phases of activity along roughly similar directions’. Also Mack et al. (1998), after a study of 5 nearby *giant* radio galaxies, argued that those sources are so huge because of their low-density environment and not because of old ages. A similar conclusion was drawn by Cotter (1998) after his study of a sample of high-redshift 7C *giants*. He found those sources to be not old and of similar kinetic powers of the jet as normal-size 3C sources. But the densities of their surrounding medium was found much lower than those around most of 3C sources (Rawlings & Saunders 1991). Ishwara-Chandra & Saikia (1999) compiled a sample of more than 50 known *giant* sources (many of them being of FRI-type morphology) and compared some of their properties with those of a complete sample of 3CR sources ‘to investigate the evolution of giant sources, and test their consistency with the unified scheme for radio galaxies and quasars’. They concluded that the location of *giants* on the power-linear size ($P - D$) diagram may suggest that the largest sources have evolved from the smaller sources. Finally, in the recent extensive study of 26 *giant* radio galaxies by Schoenmakers et al. (2000), the authors

argued that those galaxies ‘are both old sources, in term of their spectral age, and are situated in a relatively low-density environment, but also that neither of these two properties are extreme. Therefore, their large size probably results from a combination of these properties’.

From the above results, it is clear that the phenomenon of the *giant* radio sources is still open to further research. Therefore, in this paper we analyse whether observed properties of *giant* radio galaxies can be explained by a model of the dynamical evolution of classical double radio sources in cosmic time, and what factor (if there is a one) is primarily responsible for the *giant* size. Two recent analytical models, published by Kaiser et al. (1997) [hereafter referred to as KDA] and Blundell et al. (1999), are very convenient for this purpose. The overall dynamics of a FR II-type source (precisely: its cocoon) in both models is based on the earlier self-similar model of Kaiser & Alexander (1997) [hereafter referred to as KA], in which the linear size is very sensitive to a density of the source environment and a rate of its evolution with cosmic time. The models of KDA and Blundell et al. differ between themselves in predictions of a time evolution of the source luminosity. In the KDA model the synchrotron radiating particles expand from the leading head into the cocoon whose pressures are in a constant ratio during the source lifetime. This ensures the constant adiabatic losses in a self-similar expansion of the cocoon with constant geometry (axial ratio). In the model of Blundell et al. the radiating particles drift out of a constant pressure hotspot region into the cocoon in which pressure decreases throughout the source lifetime. This causes that both the expansion losses and the source axial ratio steadily increase with time, inducing a faster decrease of source (cocoon) luminosity.

In this paper, synchrotron ages in a sample of *giant* sources with FR II-type (Fanaroff & Riley 1974) morphology are used to verify the dynamical time evolution of such sources predicted by the KDA model. It is chosen here for its simplicity in spite of some objections about its application to large and old sources in which an internal pressure cannot be always above the external medium pressure, as required by a self-similar model (e.g. Hardcastle & Worrall 2000). Ba-

sic physical parameters, namely the jet power Q_0 , central density of the galaxy nucleus ρ_0 , energy density and pressure in the lobes or cocoon (u_c and p_c), and total energy of the source E_{tot} are derived from the model for each of member of the sample to fit its redshift, radio luminosity, projected size, and axial ratio. Next, these physical parameters are compared with (1) the relevant parameters derived for normal-size sources in a comparison sample, and with (2) the parameters taken from observational data, i.e. the age, equipartition energy density u_{eq} , total energy U_{eq} , lobes pressure, etc., calculated under ‘minimum energy’ conditions. The observational data used are given in Sect. 2. The method of a comparative analysis of *giants* and normal-size sources is outlined in Sect. 3. The application of the dynamical model is described in Sect. 4, while in Sect. 5 results of the modelling are presented. The evolutionary tracks of the sources on the P – D and u_{eq} – E_{tot} planes are derived and confronted with the observational data in Sect. 6. In the result, we realize that a modification of the original KDA model is necessary to provide a satisfactory fits to the data. Discussion of the obtained results and final conclusions are given in Sect. 7.

2 Observational data

Similarly to the approach of Ishwara-Chandra & Saikia (1999), we have compiled a sample of 18 *giant* sources and a comparison sample of 49 normal-size sources for which their spectral age was available from the literature. Both samples are confined to FR II-type sources only. The spectral ageing data for the *giants* are taken from the papers of Saripalli et al. (1994), Klein et al. (1996), Mack et al. (1998), Schoenmakers et al. (1998, 2000), Ishwara-Chandra & Saikia (1999), Lara et al. (2000), and Machalski & Jamroz (2000). For the aim of this paper, i.e. for an observational verification of the dynamical time evolution of *giant* sources predicted by its analytical model, the comparison sample has been chosen to comprise high-luminosity (high- and low-redshift), as well as low-luminosity normal-size sources. The high-redshift (with $z \geq 0.5$) and low-redshift ($z < 0.5$) subsamples consist of 3C sources

taken from the papers of Alexander & Leahy (1987), Leahy et al. (1989), and Liu et al. (1992). All of them have $P_{178} \geq 10^{25} \text{ W Hz}^{-1} \text{ sr}^{-1}$ (other selection criteria are summarized in Liu et al.). A low-luminosity subsample comprises FR II-type sources with $P_{1.4} < 10^{24.4} \text{ W Hz}^{-1} \text{ sr}^{-1}$ (corresponding to $P_{178} < 10^{25} \text{ W Hz}^{-1} \text{ sr}^{-1}$ assuming a mean spectral index of 0.7 between 178 and 1400 MHz). A limited number of such sources with spectral ages determined have been available from the papers of Klein et al. (1995) and Parma et al. (1999). An additional criterion applied in our study was a consistence of ages or expansion velocities given in the original papers with spectral ages homogeneously estimated by us from a fitted spectrum of the sources’ cocoon using the standard ageing analysis. The use of the spectral age is justified in Sect. 3.1 where the details of our analysis are given. The wavelength-dependent observational data are taken at $\lambda = 21 \text{ cm}$ at which a large variety of radio maps are available for all the sources.

The observational data for the sample of *giant*-size and normal-size sources are given in the Appendix.

3 Method of analysis

To start a comparative analysis of *giants* and normal-size sources, we have to determine a number of physical parameters of these sources which must be connected to their dynamical evolution. All of them are derived from the observational data using some theoretical models of a classical double radio source. In this paper we consider the following parameters: (i) the spectral age, equipartition magnetic field and total energy density derived from the standard ‘ageing analysis’ of relativistic particles in a steady-state synchrotron sources (e.g. Miley 1980; Myers & Spangler 1985), and (ii) the jet power, density of the intergalactic medium and its distribution, energy densities of relativistic particles and magnetic field, pressures at a head of the jet and in the cocoon, and total energy of a source derived from the analytical KDA model.

3.1 The spectral age

A determination of the age of the radio sources is crucial to constrain the dynamical model of time evolution. A characteristic lifetime of sources can be estimated from their total energy, E_{tot} , determined under the ‘minimum energy’ consideration and the observed power dE/dt . The resultant lifetime, being rather an upper limit to the age of source, is usually greater than the synchrotron age of relativistic particles commonly determined from the spectral-ageing analysis (e.g. Alexander & Leahy 1987). However, the time-dependence of various energy losses suffered by the particles cause that different parts of the lobes or cocoon have different ages. Besides, the radiation losses (and thus a synchrotron age) depend on a history of the particle injection, a distribution of the pitch angle, etc. described by the different synchrotron models: Kardashev–Pacholczyk (KP); Jaffe & Perola (JP); or continuous injection (CI), cf. Carilli et al.(1991) for a detailed description. An attempt to minimize the discrepancies between spectral and dynamical ages has been undertaken by Kaiser (2000). His 3-dimensional model of the synchrotron emissivity of the cocoon traces the individual evolution of parts of the cocoon and provides, according to the author, more accurate estimate for the age of a source. Its application to the lobes of Cygnus A gave a very good fit to their observed surface brightness distribution.

However, since an application of the above model is confined to the sources for which their lobes are reasonable resolved in direction perpendicular to the jet axis – we cannot use it for our statistical approach to the dynamical evolution of *giant* radio sources and have to base on the standard ageing analysis. In order to estimate a spectral age of the sample sources as homogeneously as possible, we have used a spectrum of the sources’ cocoon or their two lobes, i.e. the spectrum of entire source after a subtraction of evident hot spots and bright cores emission (e.g. the core in 3C236). This spectrum, fitted at least between 151 MHz and 5 GHz, has been used to estimate a synchrotron age of the cocoon, t_{syn} , with the prescription of Myers & Spangler (1985) for the JP model. Applying their plot of spectral index be-

tween 1446 and 4885 MHz, as well as that between 151 and 1490 MHz given in Leahy et al. (1989), we were able to find the best injection spectral index and the break frequency. The resultant ages were then compared with synchrotron ages of the sources either given explicitly in the cited papers or calculated by us from the published expansion velocities (the reference papers are given in column 9 of Table A1). If the former age agreed with the latter (to ± 30 per cent), the source is included to the samples. The above procedure was necessary because usually the values published in different papers were not derived in a uniform way. On the other hand side, it assured us that our estimates are not discrepant with those of other authors. Basing on a commonly accepted assumption about a proportionality of the spectral and dynamical ages, hereafter we assume $t_{\text{dyn}} = 2t_{\text{syn}}$ (e.g. Lara et al. 2000). This age (marked by $t[\text{Myr}]$) is given in column 2 of Table A2.

3.2 The equipartition magnetic field and energy density

Also the equipartition magnetic field strength, B_{eq} , and energy density, u_{eq} , in the cocoon or the lobes of the sample sources are homogeneously calculated using the method outlined by Miley (1980), and compared with their values given in the published papers (cf. Sect. 2). Total luminosity of the cocoons has been integrated between 10 MHz and 100 GHz using their fitted radio spectrum (cf. Sect. 3.1). The volume of the cocoons is calculated assuming a cylindrical geometry with the base diameter resulting from the axial ratio determined in the radio maps (cf. the Appendix), and the length $D/\sin\theta$, where θ is an orientation angle of the jet axis to the observer’s line-of-sight. The values of u_{eq} and B_{eq} with their estimated error, calculated with assumption of the filling factor of unity and equal distribution of energy between electrons and protons, are given in columns 3 and 4 of Table A2, respectively.

4 Application of the analytical model

Below we summarize the KA and KDA dynamical models, and precise their application in our analysis. It is assumed in the model that the radio structure is formed by two jets emanating from the AGN into a surrounding medium in two opposite directions, then terminating in strong shocks, and finally inflating the cocoon. A density distribution of the unperturbed external gas is approximated by a power-law relation $\rho_d = \rho_0(d/a_0)^{-\beta}$, where d is the radial distance from the core of a source, ρ_0 is a constant density at the core radius a_0 , and β is a constant exponent in this distribution.

The half of the cocoon is estimated by a cylinder of length $L_j = D/2$ and axial ratio $R_T = AR/2$. It expands along the jet axis driven by the hot spot pressure p_h and in the perpendicular direction by the cocoon pressure p_c . In the model the rate at which energy is transported along each jet (of power Q_0) is constant through the source lifetime. The model predicts self-similar expansion of the cocoon and gives analytical formulae for the time evolution of various geometrical and physical parameters, e.g. the cocoon pressure p_c , its linear size L_j and luminosity P_ν .

However, the pressure ratio $\mathcal{P}_{hc} \equiv p_h/p_c = 4R_T^2$, implied in the original KDA paper, has later been found to seriously overestimate a value of \mathcal{P}_{hc} obtained in hydrodynamical simulations by Kaiser & Alexander (1999). Therefore, in our modelling procedure we use the empirical formula taken from Kaiser (2000):

$$\mathcal{P}_{hc} = (2.14 - 0.52\beta)R_T^{2.04-0.25\beta}. \quad (1)$$

Moreover, taking into account the relation pointed out in Sect. 5.2.3, the KDA model is modified in our paper by a subjection of R_T on age t and Q_0 .

4.1 Radio power

The radio luminosity of the cocoon P_ν is calculated in the model by splitting up the source into small volume elements and allowing them to evolve separately. The effects of adiabatic expansion, syn-

chrotron losses, and inverse Compton scattering on the cosmic microwave background radiation are traced for these volume elements independently. The total radio emission at a fixed frequency ν is then obtained by summing up the contribution from all such elements, resulting in an integral over the time [Eq.(16) in KDA]. The integral is not analytically soluable and must be calculated numerically.

The predicted radio luminosities can be used to construct evolutionary tracks of sources on the $P-D$ diagram. These tracks can be compared with the observed distribution of sample sources on this diagram, and answer the question whether *giant* sources evolve in the same way as normal-size sources, or not.

4.2 Source energetics

In our approach we neglect thermal particles, hence the overall source dynamics is governed by the pressure in the cocoon in the form $p_c = (\Gamma_c - 1)(u_e + u_B)$, where Γ_c is the adiabatic index of the cocoon, u_e and u_B are energy densities of relativistic particles and magnetic field, respectively. Both energy densities are a function of the source lifetime t . In particular, $u_B(t) \propto B^2(t) = \text{const } t^{-a}$, where $a = (\Gamma_B/\Gamma_c)(4 + \beta)/(5 - \beta)$.

Since the time evolution of the pressure p_c is known from the self-similar solution, then one can calculate the energy density in the cocoon at any specific age t :

$$u_c(t) \equiv u_e(t) + u_B(t) = p_c(t)/(\Gamma_c - 1),$$

and the total source energy: $E_{\text{tot}}(t) = u_c(t)V_c(t)$, where V_c is the cocoon volume attained at the age t :

$$V_c(t) = 2\frac{\pi}{4R_T^2}[L_j(t)]^3 \propto t^{9/(5-\beta)}. \quad (2)$$

Following KDA and Kaiser (2000) we can write:

$$E_{\text{tot}} = u_c V_c = \frac{2(5-\beta)}{9[\Gamma_c + (\Gamma_c - 1)(\mathcal{P}_{hc}/4)] - 4 - \beta} Q_0 t. \quad (3)$$

Thus, the ratio of energy delivered by the twin jets and stored in the cocoon is:

$$\frac{2Q_0t}{E_{\text{tot}}} = \frac{9\Gamma_c - 4 - \beta}{5 - \beta} + \frac{9(\Gamma_c - 1)}{4(5 - \beta)}\mathcal{P}_{\text{hc}},$$

i.e. if $\Gamma_c = \text{const}$ and $\beta = \text{const}$, this ratio is a function of the pressure ratio \mathcal{P}_{hc} only. For $\Gamma_c = 5/3$ and $\beta = 3/2$ we have

$$2Q_0t/E_{\text{tot}} = 2.7 + 0.43\mathcal{P}_{\text{hc}}. \quad (4)$$

4.3 The fitting procedure

On the basis of the above model we aim to predict the specific physical parameters of the sample *giants* and normal-size sources at their estimated (dynamical) ages. These are: Q_0 , ρ_0 , u_c , p_c , and E_{tot} . This differs from the KDA approach, who basing on available observational data, evaluated some general trends and made crude estimation of possible range of values attained by the model parameters. Following them, we adopt their ‘Case 3’ where both the cocoon and magnetic field are ‘cold’ ($\Gamma_c = \Gamma_B = 5/3$) and the adiabatic index of the jet and internal gas is also $5/3$. For the initial ratio of the energy densities of the magnetic field and the particles we use $r \equiv u_B/u_e = (1+p)/4$, with the exponent of the energy distribution $p = 2.14$.

The core radius a_0 is one of the most difficult model parameter to be set up. Even carefull 2-D modelling of a distribution of radio emission for well known sources with quite regular structures can lead to values of a_0 discrepant with those predicted by X-ray observations, the only presently available method to determine the source environment (cf. an extensive discussion of this problem in Kaiser 2000). In our statistical approach we assume $a_0 = 10$ kpc for all sources, a conservative value in between 2 kpc used by KDA and 50 kpc found by Wellman et al. (1997). In Sect. 7.1 we discuss the consequences of other possible values of this parameter. We also use a constant value of β for all sample sources. This exponent can be easily estimated from the slope of the observed relation between $\log B_{\text{corr}}/z$ and $\log t$ in Fig.2b. As it is -0.65 ± 0.04 , then $a = (-0.65 \times 2) \pm 0.08$ and $\beta = 1.09 \pm 0.20$. This slope is much flatter than $\beta = 1.9$ adopted in KDA on the basis of Canizares et al.’s (1987) paper who found that value as typical for

a galaxy to about 100 kpc from its center. The latter value was probably justified because the uncorrected for redshift relation $\log B_{\text{eq}} - \log t$ has a steeper slope of -0.98 ± 0.05 what implies $\beta = 1.96 \pm 0.21$. Thus, we take $\beta = 1.5$ for further calculations which is compatible with other estimates of this parameter (e.g. Daly 1995). Another free parameter of the model, the orientation of the jet axis in respect to the observer’s line-of-sight $\theta = 90^\circ$ is assumed for all *giants* and $\theta = 70^\circ$ for other sources. This latter value is justified by the dominance of FR II-type radio galaxies in our sample. In view of the unified scheme for extragalactic radio sources, an average orientation angle $\langle \theta_{\text{RG}} \rangle \simeq 69^\circ$ for radio galaxies only was determined by Barthel (1989).

Given the values of a_0 , β and θ , one can find the jet power Q_0 and the initial density of external medium ρ_0 for each individual sample source characterized by the observational parameters: the age t , axial ratio AR and redshift z , by fitting the jet length L_j and the luminosity of cocoon to its observed values of $D/2$ and P_ν , respectively. The above fitting procedure was done iteratively and proved to give always stable and unique solutions.

5 Results of the modelling

The fitted physical parameters for all the sample sources are given in the Appendix. Below, we analyse a range of values and distributions of the above parameters attained by the sample sources.

5.1 Jet power Q_0 and core density ρ_0

A distribution of these parameters on the $\log(Q_0)$ – $\log(\rho_0)$ plane is shown in Fig. 1a. As both parameters should be independent between themselves, we test whether the observed distribution is or is not biased by possible selection effects. The data in Table A2 implicate that Q_0 correlates, in order of a significance level of the correlation, with luminosity $P_{1.4}$, redshift z and age t . Calculating the Pearson partial correlation coefficients, we found no significant correlation between Q_0 and ρ_0 when z (or $P_{1.4}$) and t are kept constant.

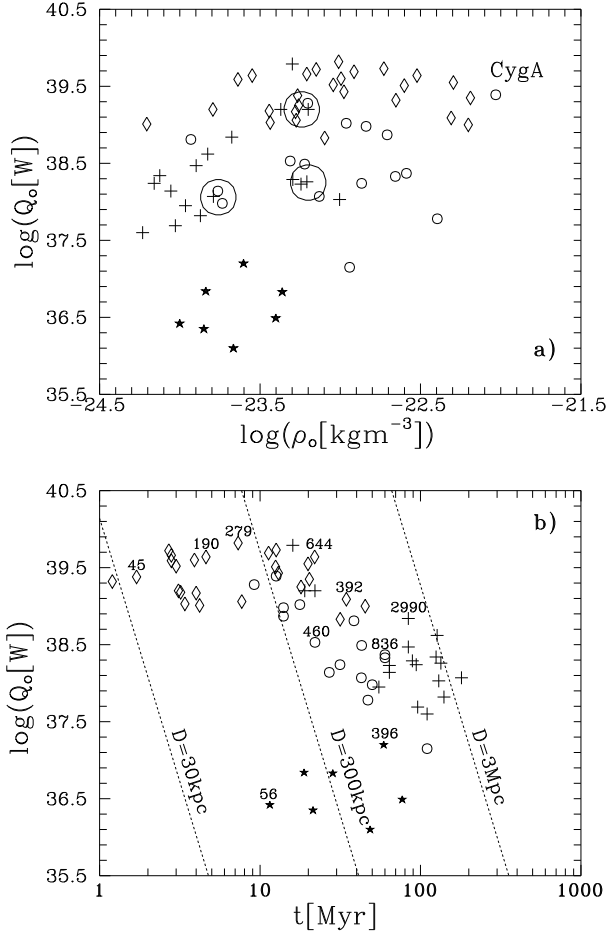


Figure 1: Plots of the jet power Q_0 **a)** against central density of the core ρ_0 ; **b)** against source age. The *giants* are indicated by crosses, high-redshift sources – diamonds, low-redshift sources – open circles, and low-redshift/low-luminosity sources – stars. The ‘clans’ of sources with similar Q_0 and ρ_0 are marked in **a)** by the large circles. The dotted lines in **b)** mark a constant linear size predicted from Eq.(6). The numbers indicate actual size of the source beneath

In view of the above, one can realise in Fig. 1a that (i) among the sources with a comparable jet power Q_0 , *giant* sources have an average central density ρ_0 smaller than a corresponding central density of normal-size sources, (ii) *giants* have at least ten times more powerful jets than much smaller low-luminosity sources of a comparable ρ_0 , and (iii) for a number of sources in the sample the derived values of their fundamental parameters Q_0 and ρ_0 are very close, while their ages are significantly different. Thus in view of the model assumptions, they may be considered as ‘the same’ source observed at different epochs of its lifetime. Such bunches of three to five sources (hereafter called ‘clans’) are indicated in Fig. 1a with the large circles. These clans have appeared crucial in a comparison of the observing data and the model predictions, and in the analysis of the *giant*-source phenomenon. More detailed analysis of these clans and their evolution is given in Sect. 6.2.

5.2 Relations between principal parameters of the sources

In this subsection we analyse a degree of correlation between the principal derived parameters of the sources: Q_0 , ρ_0 , B_{eq} , and their linear size D , axial ratio AR , redshift z , and assumed age t . For the reason that most relations between different parameters seem to be a power law, hereafter we analyse their linear correlations in the logarithmic form. Slopes of these correlations are then used to constrain the dynamical evolution model outlined in the previous Section.

5.2.1 The relations between $\log(D)$, $\log(Q_0)$, $\log(\rho_0)$, $\log(t)$, and $\log(1+z)$

A strong correlation between linear size and spectral age of 3C radio sources was already noted by Alexander & Leahy (1987) and confirmed by Liu et al. (1992). This correlation in our samples is shown in Fig. 2a. The *giant* sources do not show any departure from the correlation for the comparison sources. The same conclusion has been made by Schoenmakers et al. (2000). This means that the mean expansion velocities of those sources are similar. However,

two other details are worth to emphasize: (i) There are four high-redshift *giants* which are much younger sources than the low-redshift *giants*. Two of them are quasars. It seems that they might grow so large under some exceptional conditions. (ii) The $(\log) D - t$ relation for the low-luminosity (mostly B2) sources follows a slope of the correlation, but those sources are definitely much smaller indicating a dependence of the size and expansion velocity on luminosity.

We also note a very significant anticorrelation between redshift and age. This anticorrelation is expected because older sources at higher redshifts may fall down beyond a survey flux-limit due to the spectral and, especially inverse Compton, losses and also adiabatic expansion (cf. Blundell et al.). Since each parameter of sources in our sample correlates somehow with other parameters, in order to determine which correlation is the strongest, we calculate the Pearson partial correlation coefficients between selected parameters. All correlations are calculated between given parameters taken in the logarithmic scale (for the sake of simplicity, the ‘log’ signs are omitted in the Tables below, showing these correlations). Hereafter r_{XY} is the correlation coefficient between parameters X and Y , $r_{XY/W}$ is the partial correlation coefficient between these parameters in the presence of a third one, (W), which can correlate with both X and Y , and $P_{XY/W}$ is the probability that the test pair X and Y is uncorrelated when W is held constant. Similarly, $r_{XY/VW}$, $r_{XY/UVW}$, $P_{XY/VW}$, and $P_{XY/UVW}$ are the correlation coefficients for the correlations involving four or five parameters, and the related probabilities, respectively.

The partial correlation coefficients between selected combinations of the source parameters with the related probabilities of their chance correlation are given in Table 1.

In view of the dynamical model applied and as a result of the above statistical correlations, we realize that the linear size of a source strongly depends on both its age and the jet power, where the correlation with age is the strongest. However, the size also anti-correlates with central density of the core. That anticorrelation seems to be a weaker than the correlations with Q_0 and t and become well pronounced only when all three remaining parameters (Q_0 , t and

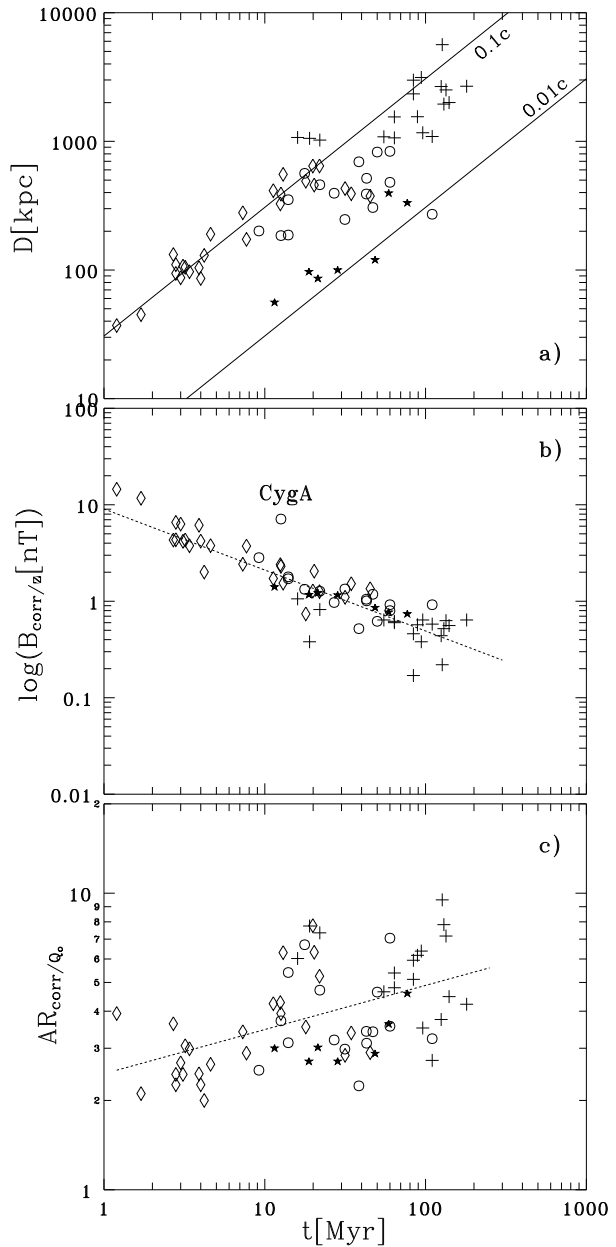


Figure 2: A distribution of selected observational parameters against the age: **a)** projected linear size D ; **b)** redshift-corrected equipartition magnetic-field strength $B_{corr/z}$ (cf. the text); and **c)** jet power-corrected axial ratio AR . The symbols indicating sources within different groups are the same as in Fig. 1. The solid lines in **a)** indicate an expansion 8 velocity of $0.1c$ and $0.01c$. The dashed lines in **b)** and **c)** indicate the linear regressions on the age axis

Table 1: The correlations between $(\log) D$ and t or Q_0 or ρ_0 when other parameters are kept constant

Correlation	$r_{XY/U}$	$P_{XY/U}$	$r_{XY/UVW}$	$P_{XY/UVW}$
	$r_{XY/V}$	$P_{XY/V}$		
	$r_{XY/W}$	$P_{XY/W}$		
$D - t/Q_0$	+0.943	$\ll 0.001$		
$D - t/\rho_0$	+0.807	$\ll 0.001$		
$D - t/1+z$	+0.840	$\ll 0.001$		
$D - t/Q_0, \rho_0, 1+z$			+0.959	$\ll 0.001$
$D - Q_0/\rho_0$	+0.013	0.918		
$D - Q_0/t$	+0.820	$\ll 0.001$		
$D - Q_0/1+z$	+0.459	$\ll 0.001$		
$D - Q_0/\rho_0, t, 1+z$			+0.884	$\ll 0.001$
$D - \rho_0/Q_0$	-0.194	0.119		
$D - \rho_0/t$	-0.080	0.525		
$D - \rho_0/1+z$	-0.086	0.492		
$D - \rho_0/Q_0, t, 1+z$			-0.745	$\ll 0.001$

z) are kept constant.

All dynamical models predict that luminosities of matured radio sources decrease with their age. Therefore, more distant sources fall through the flux-density limit of a sample sooner than nearer sources, and in any sample the high-redshift sources will be younger and more luminous than the low-redshift ones. A significant anticorrelation between Q_0 and age t , expected as a consequence of the above effect (called ‘youth-redshift degeneracy’ by Blundell et al.), is shown in Fig. 1b.

5.2.2 The relation between $\log(B_{\text{eq}})$, $\log(t)$, and $\log(1+z)$

An anticorrelation between B_{eq} and t is expected due to the basic relations for energy densities defined in Sect. 4.2. The Pearson partial correlation coefficients and the relevant probability for the chance correlation between B_{eq} and t , independent of redshift, are given in Table 2.

Table 2 confirms that there is a strong and very significant anticorrelation between the equipartition magnetic field and age of the lobes or cocoon. An apparent correlation between B_{eq} and $1+z$ is less sig-

Table 2: The correlation between $(\log) B_{\text{eq}}$, t , and $1+z$

Correlation	r_{XY}	$r_{XY/W}$	$P_{XY/W}$
$B_{\text{eq}} - t$	-0.921	-0.815	$\ll 0.001$
$B_{\text{eq}} - (1+z)$	+0.750	+0.191	0.125
$(1+z) - t$	-0.762	-0.278	0.024

nificant. A rate of decrement of the magnetic field strength is an indication of the dynamical evolution of a source (cf. Sect. 4). Thus, in order to determine a slope of the linear dependence between $\log(B_{\text{eq}})$ and $\log(t)$ independent of redshift, we have transformed the B_{eq} values from Table A.2 to a reference redshift of 0.5 using the correlation between $\log(B_{\text{eq}})$ and $\log(1+z)$. The relation between the transformed magnetic field in the sources and their age is shown in Fig. 2b.

5.2.3 The relation between $\log(AR)$, $\log(Q_0)$, and $\log(t)$

A first time (to our knowledge) axial ratios of *giant* sources were analysed and compared with those of smaller FR II-type sources by Subrahmanyam et al.

(1996), who found no difference between the axial ratios of eight *giants* and eight 3C sources with a median size of about 400 kpc. The authors did not precise what 3C sources were considered, but since all *giant* and normal sources were of comparable powers and at comparable redshifts, we presume they might be at similar ages, so the dependence of AR on time could not be visible.

In the model of Blundell et al., the axial ratio of an individual source steadily increases throughout its lifetime. Besides, that model implicates a dependence of the AR on the jet power Q_0 . The latter dependence was probably reflected by an apparent correlation between AR and 178-MHz luminosity of 3C sources noted by Leahy & Williams (1984). Taking into account the unavoidable anticorrelation between Q_0 and redshift (cf. Sect. 5.2.1), in Table 3 we have calculated the partial correlation coefficients and the related probabilities of chance correlations between AR and t , AR and Q_0 , and AR and ρ_0 when relevant combinations of the parameters t , Q_0 , ρ_0 , and $1+z$ are kept constant.

Table 3 shows a statistically significant correlations between the axial ratio and the source’s age, as well as the axial ratio and the jet power. Therefore, we have fitted a plane to the values of $\log(AR)$ over the $(\log) Q_0$ - t plane. In this and other fits of a plane performed hereafter, the ordinate values are weighted by the square of their uncertainty given in Tables A1 or A2. As a result of the above fit we found

$$AR(Q_0, t) \propto Q_0^{0.12 \pm 0.02} t^{0.23 \pm 0.04}. \quad (5)$$

Indeed, the statistical data strongly support the implication of the Blundell et al.’s model about a dependence of AR on Q_0 . A consequence of this effect for the expansion speed of the cocoon is pointed out in the next subsection. Using the above relation, one can transform the apparent AR values from Table A.1 to a reference jet power of 10^{39} W. The relation between the transformed axial ratio and age of the sample sources is shown in Fig. 2c.

5.3 Statistical expansion speed of the cocoon

The expansion speed of the cocoon along the jet axis is indirectly described by Eq.(2). Inserting $D = 2L_j$ and $AR = 2R_T$ into Eq.(2), we have $D(t) \propto (AR)^{2/3} t^{3/(5-\beta)}$. Substitution of AR from Eq.(5) and $\beta = 1.5$ into Eq.(2) gives D as a function of Q_0 and t , i.e. the expansion speed dependent on the jet power Q_0

$$D(Q_0, t) = c_1 Q_0^{0.10 \pm 0.03} t^{1.08 \pm 0.04}, \quad (6)$$

where c_1 is a constant to be empirically determined from the observed data of size and age. Expressing D in kpc and t in Myr, the constant $c_1 = (2.2 \pm 0.04) 10^{-3}$ has been found. The power exponent over t greater than unity implicates that the cocoon may expand in time with some systematic though minor acceleration. Moreover, this acceleration [according to Eq.(6)] depends on the jet power. For example, if $Q_0 = 10^{39}$ W, an average time needed to expand the cocoon from 30 to 300 kpc is about 12.1 Myr which gives an expansion speed of about $0.073c$, while about 28.2 Myr is necessary to expand it from 300 kpc to 1 Mpc which gives the speed of $0.081c$. If the jet power is two orders fainter ($Q_0 = 10^{37}$ W), these speeds are reduced to 0.047 and $0.053c$, respectively. The relation between AR and t in Eq.(5) implicates a time *deceleration* of the cocoon’s expansion if a decrease of the environment density with distance from the cluster centre is slower, i.e. if $\beta < 1.1$. However, a time evolution of the, so called, ‘clan sources’ (Sect. 6.2) seems to support the possibility of a slow acceleration in their case.

A distribution of the sample sources on the $\log Q_0$ - $\log t$ plane (Fig. 1b) shows a dramatic discrepancy between the observed large size and derived short lifetime of three *giants*: 3C274.1, 3C292, and 0437-244. They are three of four high-redshift *giant* sources in our sample. If their ages are real, they must expand with the highest velocity of about $0.2 \sim 0.25c$ (cf. also Fig. 2a). More extensive discussion of the above effect is given in Sect. 7.3.

Table 3: The correlations between (log) AR and t or Q_0 or ρ_0 when other parameters are kept constant

Correlation	$r_{XY/U}$	$P_{XY/U}$		
	$r_{XY/V}$	$P_{XY/V}$		
	$r_{XY/W}$	$P_{XY/W}$	$r_{XY/UVW}$	$P_{XY/UVW}$
$AR - t/Q_0$	+0.625	$\ll 0.001$		
$AR - t/\rho_0$	+0.456	$\ll 0.001$		
$AR - t/1+z$	+0.493	$\ll 0.001$		
$AR - t/Q_0, \rho_0, 1+z$			+0.517	$\ll 0.001$
$AR - Q_0/t$	+0.562	$\ll 0.001$		
$AR - Q_0/\rho_0$	+0.116	0.353		
$AR - Q_0/1+z$	+0.447	$\ll 0.001$		
$AR - Q_0/t, \rho_0, 1+z$			+0.424	$\ll 0.001$
$AR - \rho_0/t$	+0.357	0.003		
$AR - \rho_0/Q_0$	+0.180	0.148		
$AR - \rho_0/1+z$	+0.290	0.018		
$AR - \rho_0/t, Q_0, 1+z$			+0.186	0.142

5.4 Pressure and energy of the cocoon

In the model, energetics of the radio source is governed by the jet power Q_0 , adiabatic index Γ_c , and the pressure ratio \mathcal{P}_{hc} . Since Γ_c is assumed constant for all the sources and Q_0 is constant for a given source, the energy of the cocoon u_c and its total energy E_{tot} are determined by p_c attained by the source at age t . The cocoon pressure of the sample sources is plotted against Q_0 in Fig. 3a. It is clearly seen that the *giants* have the lowest cocoon pressure and, hence, the lowest energy density among all sources in the sample. As p_c decreases with t , and the size of source (cocoon) D increases with t , we have calculated the partial correlation coefficients for the correlation between $\log(p_c)$ and $\log(Q_0)$ at constant t or constant D . In a result, this correlation in our sample is much stronger for $D=\text{const}$ ($r_{XY/W} = +0.969$) than that for $t=\text{const}$ ($r_{XY/W} = +0.379$). Therefore, the lines of constant D in Fig.3a almost perfectly agree with actual sizes of the sources. The vertical lines indicate the time axis for members of the clans introduced in Sect. 5.1 and whose dynamical evolution is analysed in Sect. 6.2 and 6.3.

In Fig. 3b, a total energy of the cocoon E_{tot} is plot-

ted against Q_0 . It shows that the energy contained in *giant* sources spans the same range of values as does energy of normal-size sources in spite of their redshift, luminosity or age. This implicates that the decrease of energy density in time is compensated by a parallel increase of the source (cocoon) volume. Only the low-luminosity sources have energies much smaller. Imagining a division of the $\log(E_{tot})$ - $\log(Q_0)$ plane into some quadrants, the *giant*, and normal-size low-redshift and high-redshift sources are in a quadrant with $Q_0 > 10^{37.5}$ W and $E_{tot} > 10^{52.5}$ J, while the low-luminosity low-redshift radio galaxies are in the quite opposite quadrant with $Q_0 < 10^{37.5}$ W and $E_{tot} < 10^{52.5}$ J. Since the relation between E_{tot} and Q_0 at constant t , dependent only of \mathcal{P}_{hc} , is very high (the corresponding partial correlation coefficient equals to +0.991), the dotted lines in Fig. 3b indicating a constant age of sources also agree very well with the data. All *giants* but four high-redshift ones have the highest lifetime.

Now, analysing how the energetics of the sources relates to the core density ρ_0 , we found that a pressure in the cocoon p_c (thus the energy density u_c as well) also significantly depends on ρ_0 . A distribution of the sample sources on the $\log(u_c)$ - $\log(\rho_0)$ plane

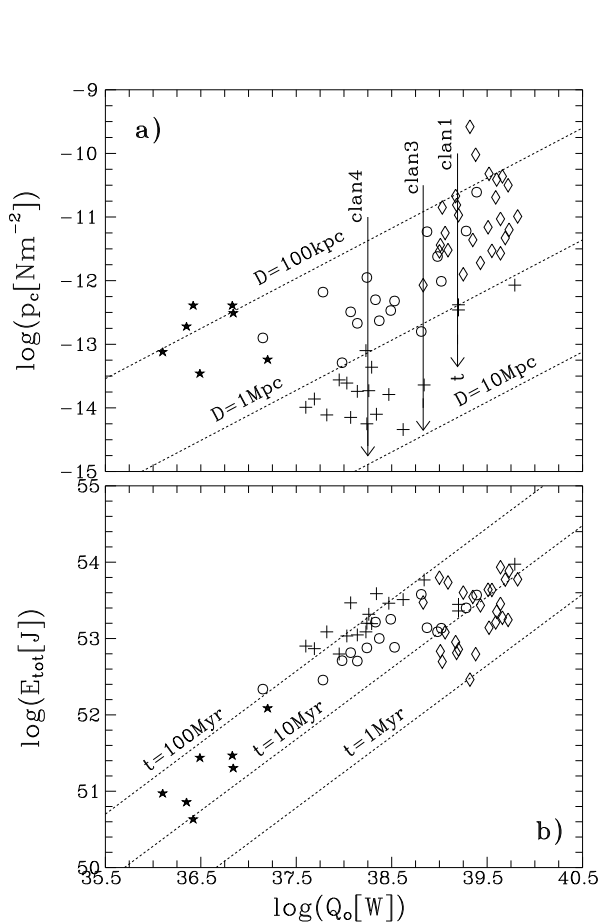


Figure 3: A distribution of modelled parameters against the jet power: **a)** the cocoon pressure p_c ; **b)** the total energy of the cocoon E_{tot} . The symbols indicating sources within different groups are the same as in Figs.1 and 2. The dotted lines mark in **a)** a constant linear size of source from the correlation $\log p_c = (-1.79 \pm 0.04) \log D[\text{kpc}] + (0.76 \pm 0.02) \log Q_0[\text{W}] - (36.9 \pm 0.9)$, in **b)** – a constant age from the correlation $\log E_{\text{tot}} = (0.90 \pm 0.03) \log t[\text{Myr}] + (0.94 \pm 0.02) \log Q_0[\text{W}] + (15.6 \pm 0.5)$. Three vertical lines in **a)** indicate time axes passing through members of the ‘clans’ of sources with very close values of Q_0 and ρ_0 (cf. the text)

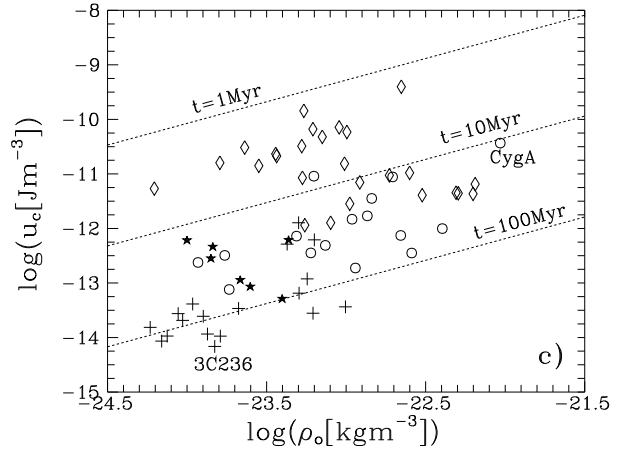


Figure 4: Energy density of the cocoon u_c against the central core density ρ_0 . The symbols – as in Fig.3. The dotted lines indicate a constant age from the statistical correlation in the sample: $\log u_c = (-1.87 \pm 0.04) \log t[\text{Myr}] + (0.80 \pm 0.04) \log \rho_0 + (9.3 \pm 0.9)$

is shown in Fig. 4. Although the correlation coefficient between $\log(u_c)$ and $\log(\rho_0)$ in Fig. 4 is only $+0.548$, a calculation shows that this direct correlation is smoothed by other correlations between the parameters u_c , ρ_0 , t , and $1+z$. The partial correlation coefficient for the correlation between $\log(u_c)$ and $\log(\rho_0)$, when t and $1+z$ are constant, equals to $+0.932$. Therefore the dotted lines of constant age in Fig. 4 again corresponds very well to the actual ages of the sources. On this plane giant sources occupy an area of the lowest values of u_c and ρ_0 .

5.5 Energy ratio $2Q_0t/U_{\text{eq}}$

The ratio of total energy supplied by twin jets during the lifetime of a source ($2Q_0t$) and its energy stored in the cocoon, derived from the data under the equipartition assumption, $U_{\text{eq}} = u_{\text{eq}}V_c$, allows another test of the dynamical model predictions, and is given in column 9 of Table A2. This ratio vs. the cocoon axial ratio AR is plotted in Fig. 5. The uncertainties of both values are marked by error bars on some data points. The solid curve indicates the model prediction from Eq.(4), while the dashed curve shows the

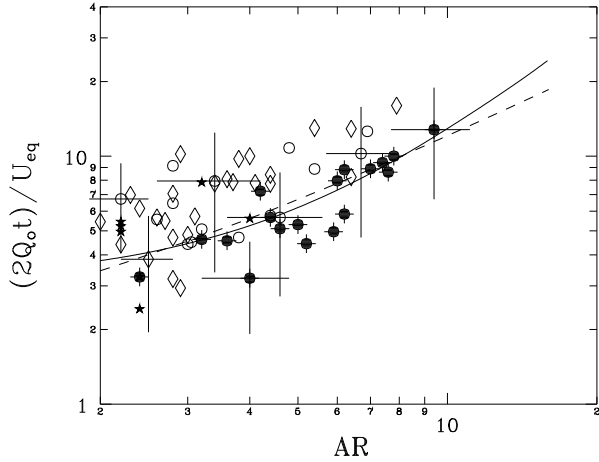


Figure 5: Ratio of the total energy supplied by twin jets and energy stored in the cocoon against its axial ratio AR . The large uncertainties of both parameters are marked by error bars for a few sources. Here the giant sources are marked with filled circles. The solid curve indicates the model prediction from Eq.(4); the dashed curve shows the best fit to weighted data

best fit to the weighted data. The observed trend fully corresponds to the model prediction. However, the derived values of $2Q_0 t / U_{\text{eq}}$, i.e. the reciprocal of an efficiency factor by which the kinematic energy of the jets is converted into radiation, is much higher than ≈ 2 , a value usually assumed in a number of papers. This aspect is discussed in Sect. 7.4.

5.6 The correlation of the cocoon pressure with age and redshift

In our statistical analysis we have noted a significant correlation between the cocoon pressure and age of sources. But age also correlates with redshift, so we have calculated the partial correlation between these parameters. Since dynamical age of sources in our sample seems to be reliably estimated, we can show that the cocoon pressure p_c very weakly depends on redshift but very strongly upon the source age. The partial correlation coefficients between p_c , t , and $1+z$ (all values in logarithmic scale) are given in Table 4.

Table 4: The correlation between $(\log) p_c$, t , and $1+z$

Correlation	r_{XY}	$r_{XY/W}$	$P_{XY/W}$
$p_c - t$	-0.924	-0.817	$\ll 0.001$
$p_c - (1+z)$	+0.771	+0.267	0.300
$(1+z) - t$	-0.762	-0.206	0.097

Thus, Table 4 shows that the apparent correlation between the cocoon pressure and redshift is caused by the stronger correlations between the pressure and age, and between the age and redshift. Fitting a plane to the values of $\log p_c$ over the $(\log) t - (1+z)$ plane we found

$$\log p_c = (-1.79 \pm 0.15) \log t [\text{Myr}] + (1.56 \pm 0.65) \log(1+z) - (10.0 \pm 0.30).$$

Therefore, one can transform the pressure values either to a fixed age or to a constant redshift. The plot of cocoon pressures transformed to $z = 0.5$ [$p_{\text{corr}/z}$] versus age t is shown in Fig. 6a, while the pressures transformed to $t = 10$ Myr versus $(1+z)$ [$p_{\text{corr}/t}$] – in Fig. 6b. These plots well illustrate very different partial correlation coefficients $r_{XY/W}$ given in Table 4. The above result put a new insight into a cosmological evolution of the IGM and is discussed in Sect. 7.5.

6 Evolutionary tracks of sources

The KDA model enables one to calculate evolutionary tracks of some secondary parameters of radio sources if their primary parameters Q_0 and ρ_0 are given. In the papers of KDA and Blundell et al. the tracks of radio luminosity P versus linear size D were derived for imaginary sources with assumed values of Q_0 , ρ_0 , a_0 , β , and z .

In our approach we are able to calculate such evolutionary tracks for actual sources. In Sect. 5.1, the ‘clans’ of sources have been pointed out, i.e. the sources with very close values of both fundamental parameters: Q_0 and ρ_0 , and evidently different ages and axial ratios. Since the dynamical model assumes

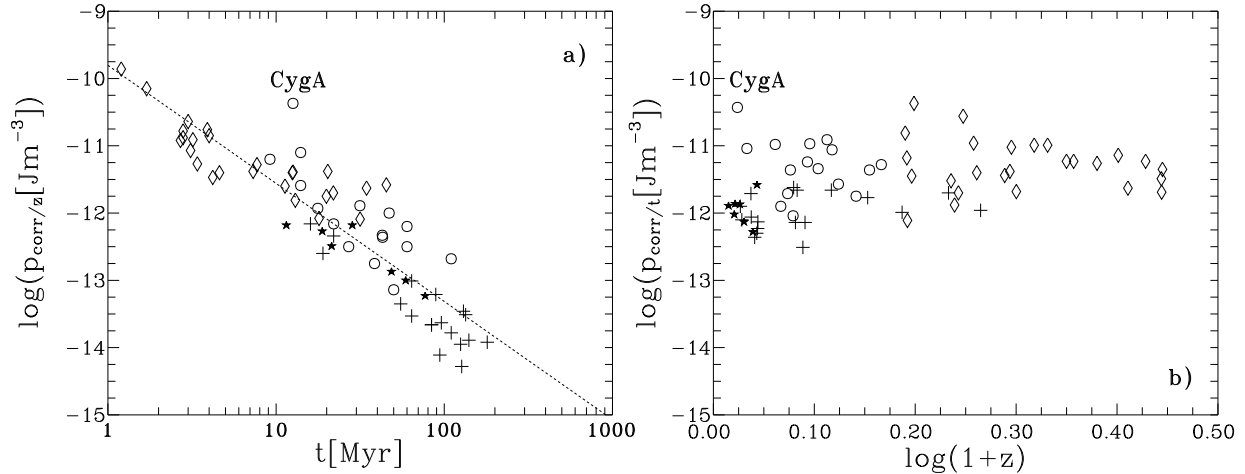


Figure 6: **a)** Cocoon pressure transformed to the constant redshift of 0.5 against age of the sample sources. The best linear fit is indicated by the dotted line; **b)** The same pressure transformed to the constant age of 10 Myr against redshift

constant jet power during a source lifetime, and a nucleus density ρ_0 is *a priori* constant, members of such clan can be considered as ‘the same’ source observed at a number of different epochs throughout its life. The observed parameters of these members can verify predictions of the model. However, fits of the tracks predicted with the original KDA model to the observed parameters of sources have appeared unsatisfactory. Much better fits of the modelled tracks to observational data of the ‘clan’ members are found with the cocoon axial ratio evolving in time, as reported in Sect.5.3. This, in turn, implicates a time evolution of the pressure ratio \mathcal{P}_{hc} . Indeed, substitution of Eq.(5) into Eq.(1), one has (for $\beta = 3/2$, and where Q_0 is in watts and t in Myr)

$$\mathcal{P}_{\text{hc}}(t) \approx 2.3 \cdot 10^{-8} Q_0^{0.20 \pm 0.03} t^{0.38 \pm 0.05}. \quad (7)$$

6.1 The clans

We found 6 clans consisting of 3, 4 or 5 sample sources fulfilling a selection criterion, namely that the fitted values of Q_0 and ρ_0 do not differ between themselves by more than 30 per cent. Also redshift of members should be comparable, however in our small sample

we have accepted the redshift ratios up to about 3. Three of six clans are marked in Fig. 3a. Their members are listed in Table 5.

Table 5: Members of the selected clans

	Clan1	Clan3	Clan4
$\langle \lg Q_0 \rangle$	39.26	38.84	38.21
$\langle \lg \rho_0 \rangle$	-23.24	-23.35	-23.22
redshift range	1:2.3	1:2.3	1:3.4
members	3C263.1	3C166	3C319
	3C289	3C334	1025-224
	3C411	1012+488	0136+396
	3C272	0821+695	3C326
	3C274.1		

The members are ordered according to their increasing age. In all three clans that increase of age is accompanied with an increase of the size and total energy of the members, altogether with a decrease of their luminosity and energy density. This qualitative observational behaviour, concordant with the model expectations, is quantitatively presented in the following subsections.

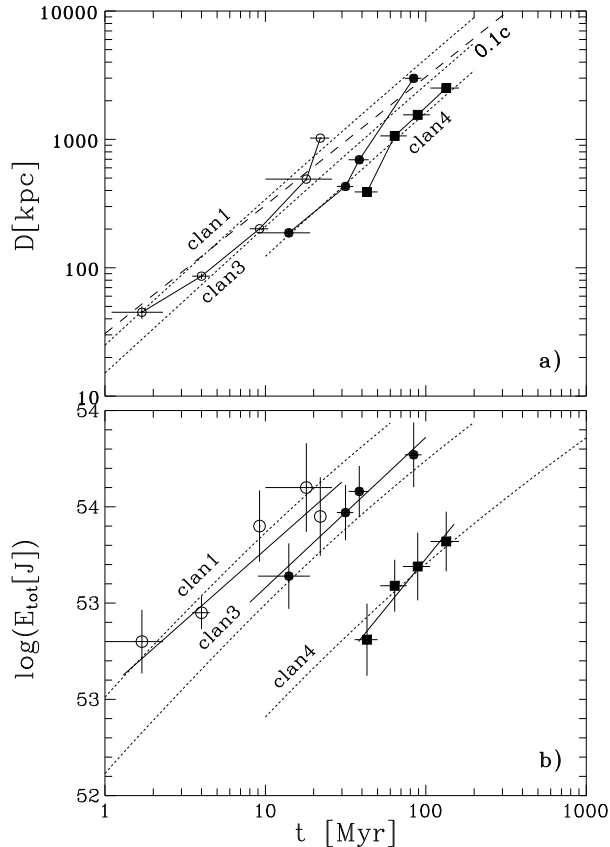


Figure 7: **a)** Time evolution of the size of a fiducial source for each of the three observed clans (dotted lines). The dashed line indicates a constant advance speed of $0.1c$; **b)** Evolution of the total energy of a fiducial source for each of the clans. The shorter solid lines show the best linear fit to the data points

6.2 Time evolution of the clans

In order to check whether observed parameters of the members of a given clan are consistent with a time evolution derived from the model, a fiducial source has been determined for each clan. This fiducial source has Q_0 and ρ_0 equal to the mean value of these parameters in a given clan and the evolving axial ratio of the cocoon, as given by Eq.(5). For each of the clans, a time evolution of its size $D(t)$, luminosity $P(t)$, energy density $u_c(t)$, and total energy $E_{tot}(t)$ have been calculated. The predicted $D(t)$ tracks for the three clans are shown in Fig. 7a with the dotted lines overlaid on the solid lines connecting members of each clan drawn with different symbols. The data points are shown with error bars (the errors in size are usually smaller than the vertical size of symbols). The dashed line indicates $D(t)$ for the constant advance speed of $0.1c$. The higher slopes of the modelled tracks in respect to this constant speed seem to confirm accelerating a little expansion of the cocoon in the investigated clans (as deduced in Sect. 5.4), however the effect is of low significance because of uncertainties of the age.

The predicted evolution of the total energy for the three clans is shown in Fig. 7b with the dotted lines. The solid lines indicate the best linear fit to the data points. A correspondence between the modelled $E_{tot}(t)$ and the data points is satisfactory.

6.3 The tracks $\log P - \log D$

The evolutionary tracks for the three clans are shown in Fig. 8 with solid curves. The markers of the same time on these tracks are connected with a dotted line. The members of separate clans are indicated by different symbols. A numer in vicinity of each symbol indicates actual age of the corresponding source in Myr. The dashed curves show the relevant track calculated from the original KDA, model, i.e. with a constant AR taken as the mean of axial ratios in a given ‘clan’. It is clearly seen that the evolving AR much better fits the observed changes of P and D . The further discussion about these tracks is given in Sect. 7.6.

6.4 The tracks $\log(u_{\text{eq}})$ – $\log(E_{\text{tot}})$

The model also allows to predict the evolution of a source on the energy density–total energy plane. These tracks are shown in Fig. 9 with solid curves. As in Fig. 8, the time markers are connected with dotted lines, and the member sources of each clan are indicated with the same symbols. Note that the ordinate of every source is its equipartition energy density derived from the observational data, while the modelled tracks show the *fitted* cocoon energy density. This is an additional argument that the modified model satisfactory reproduce the data. In Fig. 9, an uncertainty of a value of both parameters is shown by the error bars, where error of u_{eq} is given in Table A2 and error of E_{tot} is estimated from the error of source volume. Again, the numbers mark actual age of the corresponding source. The straight dashed lines indicate the tracks computed with the constant AR . It is worth to emphasize that the predicted evolutionary u_c – E_{tot} tracks are steeper and curved in respect to those expected from the original KDA model. This effect, related to a rate of adiabatic losses and inflation of the cocoon, is discussed in Sect. 7.6.

7 Discussion of the results and conclusions

7.1 Influence of fixed model parameters on the model predictions

Basic physical parameters of the radio sources derived in this paper, i.e. jet power Q_0 , central density ρ_0 , and cocoon pressure p_c , are in principle dependent on assumed central core radius, exponent in the external gas distribution, adiabatic indices of electrons and magnetic field, as well as on orientation of the jet axis towards the observer. In application of the KA model we have assumed the same values of these parameters for all sample sources. This assumption can only be valid in our statistical analysis of the evolutionary trends in the whole FR II-type population but not for individual sample sources. In particular, we have adopted $a_0 = 10$ kpc and $\beta = 1.5$, respectively. Taking up a lower core radius, e.g. $a_0 = 2$ kpc, and

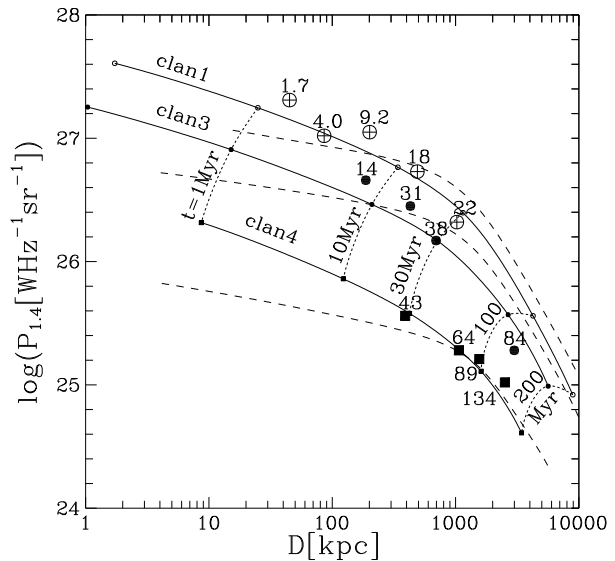


Figure 8: Evolutionary P – D tracks fitted for three clans of sources with evolving axial ratio AR (solid curves). The markers of the same predicted age on each curve are connected with dotted lines. The members of each clan are marked with different symbols as those in Figs. 7a and 7b. Their actual age is indicated by a number behind the symbol. The dashed curves indicate relevant tracks but calculate with a constant AR , as in original KDA model

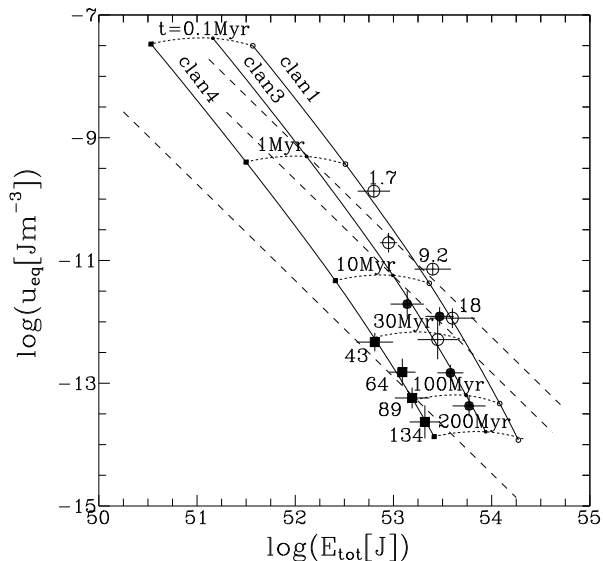


Figure 9: Tracks of evolving energy fitted for the three clans. All the lines and symbols are the same as in Fig. 8.

keeping $\beta = 1.5$ will result in increase of the modelled density of the core ρ_0 by roughly one order of magnitude, while other modelled parameters will not be changed. Oppositely, a lower density gradient, e.g. $\beta = 1.1$, will lower ρ_0 approximately 1.5 ~ 6 times. In this case however, the jet power will be increased about a few percent and accordingly will be changed the pressure and energy density in the cocoon. A relativistic equation of state for the magnetic field does not change our results significantly, unless the KDA ‘Case 1’ ($\Gamma_c = \Gamma_B = 4/3$) is adopted. However, this case, i.e. when both, the cocoon and the magnetic field energy, have a relativistic equation of state, is unlikely for our sample sources. Therefore, we argue that the results discussed below are not significantly biased by a selection of particular set of the model parameters.

7.2 A cause of extremal linear size

In view of the KA and KDA analytical models of dynamical evolution of FR II-type radio sources, many

such sources can evolve into a stage characterized by the linear size exceeding 1 Mpc. An access to this stage depends on a number of the model parameters: jet power Q_0 , its Lorentz factor γ_{jet} , adiabatic indices of the cocoon material and magnetic field, Γ_c and Γ_B , respectively, as well as a core radius a_0 , external gas density ρ_0 , and exponent of its distribution β . For a given set of these parameters, the model allows to determine whether an evolving source will reach or not the size of 1 Mpc, and if so, at what age. From this point of view, *giant* sources should be the oldest ones.

In this paper we have confronted the model predictions with the observational data on *giant*-size and normal-size FR II sources. Our analysis strongly suggests that there is not a single evolutionary scheme governing the size development. An old age or a low external density alone is insufficient to assure extremely large linear extent of a source, both are necessary together with a suitable power driven from AGN by the highly relativistic jets. About 83 per cent of *giants* in our sample possess the projected linear size over 1 Mpc owing to statistically old age, low or moderate density of the external medium, and high enough power of their jets. The remaining 17 per cent (3 sources) are high luminosity radio galaxies at redshifts $z > 0.4 \sim 0.5$ and ages from 15 to 25 Myr which are typical for normal-size sources. The jet power of these galaxies is high enough to compensate for a higher ram pressure in a denser surrounding environment and higher energy losses during the cocoon expansion. The jet power of *giants* is not extreme, so several FR II-type sources having that Q_0 can potentially achieve very large size after a suitable long time. According to our results (cf. Fig. 2a), these potential *giants* should have $Q_0 > 10^{37.5}$ W and be situated in environment with $\rho_0 < 10^{-23}$ kg m $^{-3}$.

The above scenario is not caused by a selection effect. We show that there are low-luminosity sources which lay in the parts of $\log Q_0 - \log \rho_0$ (Fig. 2a) and $\log E_{\text{tot}} - \log Q_0$ (Fig. 3b) planes completely avoided by *giant* sources. They diverge from *giants* and even normal-size powerful sources by having low jet power $Q_0 < 10^{37.5}$ W and total energy $E_{\text{tot}} < 10^{52.5}$ J, thus are not expected to ever reach the giant size. It is worth to note that some of them already have an age

comparable to that of typical *giants*, in accordance with the model expectations.

7.3 Acceleration of the cocoon expansion speed

The statistical analysis in Sect. 5.4 suggests that for $\beta > 1.1$ the power exponent of age t in Eq.(6) is greater than unity, thus the cocoon expansion along the jet axis may accelerate in time. This effect is also seen in the time evolution of *fiducial* sources well representing the ‘clans’ of a few actual sample sources in which each source in the ‘clan’ with almost identical values of Q_0 and ρ_0 is observed at different age (cf. Sect. 6.2 and Fig. 7a).

Below we argue that the above effect may be real and some arguments come from the well known hydrodynamical considerations. Beginning from Scheuer (1974), it is commonly accepted that the ram pressure of the external gas behind the head of jet is $\rho_d \mathcal{V}_h^2 \approx Q_0 / (A_h v_{\text{jet}})$, where ρ_d is the external density (at the radial distance d), \mathcal{V}_h is the head expansion speed, A_h is the head working surface, and the jet bulk velocity v_{jet} is commonly assumed to be close to the light speed c . Therefore, \mathcal{V}_h is a function the root square of the ratio Q_0 / ρ_d and the reciprocal of a linear size (diameter) of the working area. Q_0 / ρ_d simply represents an effectiveness of the jet propagation across the surrounding medium. We can consider this ratio at the core radius a_0 and at the source leading head where it is Q_0 / ρ_0 and $Q_0 / \rho_{\text{end}} = Q_0 / \rho_0 (D / 2a_0)^{-\beta}$, respectively. Both ratios are derived from the model. Values of the first ratio for *giant* sources are not much different from those for other sample sources being little smaller than corresponding values for high-redshift sources, comparable with those for low-redshift sources, and evidently higher from those for low-luminosity ones. The second ratio, as a function of D^β , is the highest for *giant* sources.

The area of A_h at a given radius from the AGN centre can be determined from high-resolution observations of the hotspots. For example, VLBI observations of selected ‘compact symmetric objects’ (CSO), possibly progenitors of classical double FRI and/or FRII sources give a linear size of the working area

of about a few parsecs at a radius of about 50~100 pc (cf. Owsianik et al. 1998). Many VLA observations of hotspots in sources of size 10~20 kpc show that their sizes are not larger than about 500 pc, while the hotspot sizes in the lobes of large sources do not exceed 15 kpc. Schoenmakers et al. (2000) in their study of *giant* radio sources have assumed a typical hotspot size of 5 kpc at a radius of 0.5 ~ 1 Mpc. After a discovery of the third largest radio galaxy J1343+3758 (1343+379 in Tables A1 and A4), Machalski & Jamrozy (2000) determined a working surface with diameter of about 13 kpc in one of its lobes.

From the data in our subsample of *giant* sources we have $\langle Q_0 / \rho_0 \rangle = 10^{61.9 \pm 0.13} \text{ W m}^3 \text{ kg}^{-1}$ and $\langle Q_0 / \rho_{\text{end}} \rangle = 10^{64.9 \pm 0.19} \text{ W m}^3 \text{ kg}^{-1}$. Dividing the first ratio by $A_h \approx 2 \cdot 10^{38} \text{ m}^2$ (the working area for hotspot diameter of 0.5 kpc) and the second ratio by $A_h \approx 8 \cdot 10^{40} \text{ m}^2$ (for hotspot diameter of 10 kpc), we obtain \mathcal{V}_h of about 0.12 and 0.19 c , respectively. Although these speeds are, at least, two times higher than those expected from the total linear extent of sources and their estimated ages (cf. Fig. 1a), their proportion agrees with proportions found in Sect. 5.4. The above speeds, too high in respect to an upper limit of \mathcal{V}_h (i.e. the quotient $D/2t$), can be caused by either too high modelled jet power or too low internal density of the core and of the cocoon at its end. An adjustment of β will not work because some increase of β can compensate for too low ρ_0 , but will dramatically lower ρ_{end} . Since the values of A_h adopted for this calculation may be rather overestimated than underestimated, only a decrease of Q_0 can fit the observed expansion speeds. Even authors of the KDA paper already noted that Q_0 derived from their model is an order of magnitude stronger than a jet power (Q^{js}) calculated from the values given by Rawlings & Saunders (1991). Indeed, neglecting a thermal gas in the cocoon and taking $\Gamma_c = 5/3$ and $\beta = 3/2$ (as in our calculations), one can found $Q_0 / Q^{\text{js}} = 1.7 \sim 5.5$ depending on the value of \mathcal{P}_{hc} . Also Lara et al. (2000), assuming an upper limit temperature of the ambient gas around the high-redshift *giant* galaxy 0821+695 and deriving the source expansion speed, have determined its jet power of $(7.1 \sim 9) \cdot 10^{37} \text{ W}$ which is almost ten times weaker than our value of

6.9 10^{38} W for that source (cf. Table A2). A suspicion that the jet power determined from the KA model may be too high is supported by much higher than usually assumed ratios of energy $2Q_0t/U_{\text{eq}}$.

7.4 Energy budget

In a number of studies of *giant* radio sources (e.g. Parma et al. 1996; Schoenmakers et al. 1998) a fraction of the total jet energy wasted for adiabatic expansion of the cocoon is usually assumed to be about 0.5 and used to estimate the jet power Q_0 if the age of a source is known (almost always from the spectral ageing analysis). In the KA model the energy stored in the source (cocoon) is

$$E_{\text{tot}} \approx \int \{Q_0 dt - (p_c d[V_c(t)] + p_h d[V_h(t)])\}$$

where $p_c dV_c + p_h dV_h$ is a work done to expand the cocoon, and p_h and V_h are the hotspot pressure (cf. Sect. 4) and its volume, respectively. If V_h is neglected, the expansion work will be $\approx 0.5 Q_0 t$; if not, it is dependent on the pressure ratio \mathcal{P}_{hc} as shown in Sect. 4.2.

In spite of a supposed uncorrectness (possibly a systematic overestimation) of the jet power derived from the model, the data in our sample fully confirm a dependence of the energy ratio $2Q_0t/U_{\text{eq}}$ on the cocoon axial ratio AR , and imply an increase of the fraction of jet energy lost for the adiabatic slender expansion of the cocoon volume in time. However, the data also suggest that for a constant AR (a given geometry of cocoon), *giants* tend to have a smaller ratio of $2Q_0t/U_{\text{eq}}$ than normal-size sources, i.e. less energy of the jets was converted into adiabatic expansion of the cocoon. This may indicate a lower pressure of the external medium surrounding the *giant* sources than that around shorter ones. That external pressure may be in the thermal equilibrium with internal pressure in a large part of the cocoon.

7.5 External pressure of the surrounding medium and its evolution

A non-relativistic uniform intergalactic medium (IGM) in thermal equilibrium filling an adiabatically expanding Universe should have an electron pressure evolving with redshift $p_{\text{IGM}} = p_{\text{IGM}}^0 (1+z)^5$. The advancing hotspots of FR II-type radio sources are probably confined by ram pressure of the IGM. *Giant* sources, with their lobes extended far outside a cluster halo, have the lowest values of p_c and may be useful to determine an upper limit of p_{IGM} . Using a small sample of *giant* sources, Subrahmanyan & Saripalli (1993) limited its local value to $p_{\text{IGM}}^0 \approx (0.5 \sim 2) 10^{-15} \text{ N m}^{-2}$. A further study was undertaken by Cotter (1998) who, using a larger sample of 7C giants with sources out to redshift of about 0.9, confirmed a strong dependence of the lowest p_c and redshift in agreement with a $(1+z)^5$ relation. This observational result has been critically discussed by Schoenmakers et al. (2000), who have considered possible selection effects in the Cotter's analysis, and concluded that there was not evidence in their own sample for a cosmological evolution of p_{IGM} . However, they also declare that this hypothesis cannot be rejected until some low-pressure high-redshift sources are found.

In all above analyses the age of sources was out of consideration. The very significant correlation between p_c and t , shown in Sect. 5.7, strongly suggests that the intrinsic dependence of age on redshift but not the Malmquist bias is mainly responsible for the apparent correlation between p_c and $1+z$. Nevertheless, we agree with the Schoenmakers et al.'s conclusion that until *giant* sources with internal pressures in their lobes $p_c < 2 10^{-15} \text{ N m}^{-2}$ at redshifts of at least 0.6 \sim 0.8 are not discovered, the IGM pressure evolution in the form $p_{\text{IGM}} \propto (1+z)^5$ cannot be rejected.

Most *giants* in our sample, but four high-redshift ones, reveal the lowest pressure in their cocoons. Sharing Subrahmanyan & Saripalli's arguments, we can expect those cocoon pressures are indicative of an upper limit to the present-day external pressure of the IGM, p_{IGM}^0 . Taking into account the lowest values of p_c (cf. Figs. 3a and 5a), we found $p_{\text{IGM}}^0 < 2 10^{-15}$

N m^{-2} in accordance with their value. It is worth to emphasize that the above results are obtained from the analytical model assuming the energy equipartition (cf. Sect. 4.3). This may not be the case in every part of the source (cocoon). Hardcastle & Worrall (2000) estimated gas pressures in the X-ray-emitting medium around normal-size 3CRR FRII radio galaxies and quasars, and found that, with few exceptions, the minimum pressures in their lobes, determined under equipartition conditions, were well below the environment pressures measured from old ROSAT observations. Therefore, they argued after an additional contribution to the internal pressure in lobes of those sources including pressure from protons, magnetic fields differing from their minimum-energy values, or non-uniform filling factors. Nevertheless, the diffuse lobes of *giants*, extending farther off from a host galaxy than a typical radius of high-density X-ray-emitting cluster gas, may be in equilibrium with an ambient medium whose emissivity is not directly detectable.

7.6 Dynamical evolution of individual sources

In Sections 6.3 and 6.4 we have presented the evolutionary tracks of the ‘fiducial’ sources across the P - D and $u_{\text{eq}}-E_{\text{tot}}$ planes, respectively, calculated according to our modified KDA model, and afterwards compared them with the predictions of the original KDA model. A predicted evolution of each ‘fiducial’ source, i.e. its tracks across the above planes, is verified by the age, luminosity, size, and the energy of a ‘clan’ members (cf. Sect. 6.2). Therefore, we consider those sources as an individual source observed at different lifetime epochs, and the relevant ‘fiducial’ source is its model representation.

Figs. 8 and 9 show that for each of the three ‘clans’ our tracks are steeper than those resulting from the KDA model, and much better corresponds to the observed parameters of the ‘clan’ sources. Our P - D tracks strictly resemble those published by Blundell et al., as both arise from the dynamical models accounting for not self-similar evolution of the source cocoon. This is interesting that we get similar tracks from a different approach, subsequently supporting

predictions of their model. The observed distributions of the ‘clan’ sources across the P - D and $u_{\text{eq}}-E_{\text{tot}}$ planes give further arguments after a necessity to account for evolving axial ratio of the cocoon in studies of the dynamical evolution of individual radio sources.

This is worth to emphasize a much higher potential of such analytical models than it was exploited in previous papers, namely an evolution of the energy density and total energy stored in a source (its lobes or cocoon) can be modelled and compared with observations. The tracks of our ‘clans’ across the $u_{\text{eq}}-E_{\text{tot}}$ plane are steeper than those predicted by the original KDA model for sources with constant axial ratios. Moreover, the steepening increases throughout the source lifetime. This is caused by a non-linear decline of the adiabatic losses and inflation of the cocoon in time, as well as a faster decrease of the cocoon pressure in very large sources. Quantitatively this process is evaluated by the substitution of the evolving (increasing) value of the pressure ratio $\mathcal{P}_{\text{hc}}(t)$, given by Eq.(7), into Eq.(3).

From our analysis we can conclude as follows:

(1) The data show that the source (cocoon) geometry, described by its axial ratio, depends on its estimated age. Incorporation of the cocoon axial ratio evolving with time into the analytical model of Kaiser et al. (1997) [referred in this paper as KDA], allow us to reproduce a dynamical evolution of the FRII-type radio sources better than with their original model which assumes a self-similar expansion of the cocoon of sources. Therefore we can confirm a conclusion drawn by Blundell et al. (1999) that throughout the lifetime of an individual source its axial ratio must steadily increase, thus its expansion cannot be self-similar all the time. A self-similar expansion seems to be feasible if the power supplied by the jets is a few orders of magnitude above the minimum-energy values. In other cases the expansion can only initially be self-similar; a departure from self-similarity for large and old radio sources is justified by observations of *giant* sources.

(2) Inserting a statistical correlation between axial ratio and age of the sample sources into the model, we calculate the evolutionary tracks of a few ‘fiducial’ sources across the P - D and $\rho_{\text{eq}}-E_{\text{tot}}$ planes.

Resultant luminosity, size, and energy density of a given ‘fiducial’ source, derived for different epochs of its lifetime, are then compared with relevant parameters of a few real sample sources (called a ‘clan’) having the model parameters Q_0 and ρ_0 similar and common with the fiducial source. The derived P – D tracks appear to be much steeper and better fit the observational data than those provided with the original KDA model, and are compatible with those expected from more sophisticated model of Blundell et al. (1999).

(3) In the case of ‘clan’ sources, we found a slow acceleration of the average expansion speed of the cocoon along the jet axis. This effect is predicted with the model modified as above, and is caused by a systematic increase of the ratio between hotspot and cocoon pressures (\mathcal{P}_{hc}) with the age of source and decreasing density of the external environment with $\beta > 1.1$ in its β -model. The statistics suggests that this acceleration is also dependent of the jet power.

(4) An evolution of the energetics of sources, predictable from the model, form another characteristics of their population which can be constrained by observational data.

(5) *Giant* sources do not form a separate class of radio sources, and do not reach their extreme sizes exclusively due to some exceptional physical conditions of the external medium. In average, they are old sources with high enough jet power evolved in relatively low-density environment. However, for the observed high-redshift *giants* we found their jets almost ten times more powerful than those in low-redshift ones, while the core densities of high- z and low- z *giants* do not differ so much. From the statistical point of view, we found that for sources with comparable jet power Q_0 , the size D correlates stronger with their age than anti-correlates with core density ρ_0 . For *giants* with a comparable ρ_0 and age, the size D strongly correlates with Q_0 .

(6) *Giants* possess the lowest equipartition magnetic field strength and energy density of their cocoons making a difficulty of their detection in synchrotron emission. However, the accumulated total energy is the highest and exceeds $3 \cdot 10^{52}$ W.

(7) The apparent increase of the lowest internal pressures (observed in the largest sources) with red-

shift is mainly caused by the intrinsic dependence of their age on redshift and dominates over the Malmquist bias suspected by Schoenmakers et al. (2000) as responsible for this increase. However, a cosmological evolution of the IGM cannot be rejected until *giant* sources with internal pressures in their lobes less than $2 \cdot 10^{-15}$ N m² at high redshifts are not discovered.

8 acknowledgements

We thank Dr. C. R. Kaiser for explanations of the integration procedures used in the KDA paper. This work was partly supported by the State Committee for Scientific Research (KBN) under contract PB 266/PO3/99/17.

References

- [1987] Alexander, P., Leahy J.P., 1987, MNRAS, 225, 1
- [1989] Barthel, P.D., 1989, ApJ, 336, 606
- [1996] Becker, R.H., White, R.L., Helfand, D.J., 1995, ApJ, 450, 559
- [1999] Blundell, K.M., Rawlings, S., Willott, C.J., 1999, AJ, 117, 766
- [1987] Canizares, C.R., Fabbiano, G., Trinchieri, G., 1987, ApJ, 312, 503
- [1991] Carilli, C.L., Perley, R.A., Dreher, J.W., Leahy, J.P., 1991, ApJ, 383, 554
- [1998] Condon, J.J., Cotton, W.D., Greisen, E.W., Yin, Q.F., Perley, R.A., Taylor, G.B., Broderick, J.J., 1998, AJ, 115, 1693
- [1998] Cotter, G., 1998, in "Observational cosmology with the new sky surveys"; eds.: M.N. Bremer et al., Kluwer Acad. Publ., p.233
- [1995] Daly, R.A., 1995, ApJ, 454, 580
- [1986] de Ruiter, H.R., Parma, P., Fanti, C., Fanti, R., 1986, A&AS, 65, 111

- [1974] Fanaroff, B.L., Riley, J.M., 1974, MNRAS, 167, 31P
- [2000] Hardcastle, M.J., Worrall, D.M., 2000, MNRAS, 319, 562
- [1979] Hine, R.G., 1979, MNRAS, 189, 527
- [1999] Ishwara-Chandra, C.H., Saikia, D.J., 1999, MNRAS, 309, 100
- [2000] Kaiser, C.R., 2000, A&A, 362, 447
- [1997] Kaiser, C.R., Alexander, P., 1997, MNRAS, 286, 215 (KA)
- [1999] Kaiser, C.R., Alexander, P., 1999, MNRAS, 302, 515
- [1997] Kaiser, C.R., Dennett-Thorpe, J., Alexander, P., 1997, MNRAS, 292, 723 (KDA)
- [1995] Klein, U., Mack, K.-H., Gregorini, L., Parma, P., 1995, A&A, 303, 427
- [2000] Lara, L., Mack, K.-H., Lacy, M., Klein, U., Cotton, W.D., Feretti, L., Giovannini, G., Murgia, M., 2000, A&A, 356, 63
- [1989] Leahy, J.P., Muxlow, T.W.B., Stephens, P.W., 1989, MNRAS, 239, 401
- [1984] Leahy, J.P., Williams, A.G., 1984, MNRAS, 210, 929
- [1992] Liu, R., Pooley, G., Riley, J.M., 1992, MNRAS, 257, 545
- [1983] Machalski, J., Condon, J.J., 1983, AJ, 88, 1591
- [1985] Machalski, J., Condon, J.J., 1985, AJ, 90, 5
- [2000] Machalski, J., Jamrozy, M., 2000, A&A, 363, L17
- [2001] Machalski, J., Jamrozy, M., Zola, S., 2001, A&A, 371, 445
- [1997] Mack, K.-H., Klein, U., O'Dea, C.P., Willis, A.G., 1997, A&AS, 123, 463
- [1998] Mack, K.-H., Klein, U., O'Dea, C.P., Willis, A.G., Saripalli, L., 1998, A&A, 329, 431
- [1980] Miley, G.K., 1980, ARA&A, 18, 165
- [1985] Myers, S.T., Spangler, S.R., 1985, ApJ, 291, 52
- [1998] Owsianik, I., Conway, J.E., Polatidis, A.G., 1998, A&A, 336, L37
- [1986] Parma, P., de Ruiter, H.R., Fanti, C., Fanti, R., 1986, A&AS, 64, 135
- [1996] Parma, P., de Ruiter, H.R., Mack, K.-H., van Breugel, W., Dey, A., Fanti, R., Klein, U., 1996, A&A, 311, 49
- [1999] Parma, P., Murgia, M., Morganti, R., Capetti, A., de Ruiter, H.R., Fanti, R., 1999, A&A, 344, 7
- [1991] Rawlings, S., Saunders, R., 1991, Nature, 349, 138
- [1994] Saripalli, L., Subrahmanyan, R., Hundstead, R.W., 1994, MNRAS, 269, 37
- [1974] Scheuer, P.A.G., 1974, MNRAS, 166, 513
- [2001] Schoenmakers, A.P., de Bruyn, A.G., Röttgering, H.J.A., van der Laan, H., 2001, A&A, 374, 861
- [1998] Schoenmakers, A.P., Mack, K.-H., Lara, L., Röttgering, H.J.A., de Bruyn, A.G., van der Laan, H., Giovannini, G., 1998, A&A, 336, 455
- [2000] Schoenmakers, A.P., Mack, K.-H., de Bruyn, A.G., Röttgering, H.J.A., Klein, U., van der Laan, H., 2000, A&AS, 146, 293
- [1984] Spangler, S.R., Pogge, J.J., 1984, AJ, 89, 342
- [1993] Subrahmanyan, R., Saripalli, L., 1993, MNRAS, 260, 908
- [1996] Subrahmanyan, R., Saripalli, L., Hundstead, R.W., 1996, MNRAS, 279, 257
- [1995] Urry, C.M., Padovani, P., 1995, PASP, 107, 803
- [1997] Wellman, G.F., Daly, R.A., Wan, L., 1997, ApJ, 480, 96

A Observational data and physical parameters of the sample sources

The observational data for the *giant*-size and normal-size sources are listed in Table A1. Although all columns of Table A1 are self-explanatory, some more detailed informations are given below. The overall axial ratio (AR) of the sources is determined from total intensity maps as the ratio of the entire projected source size to the average of the full deconvolved widths of the two lobes. The later are measured between 3σ contours on a radio contour map half-way between the core and the hot spots or distinct extremities of the source. The reference to the maps used is given in column 8 of Table A1. The volume of the sources is calculated assuming a cylindrical geometry with the diameter equal to the average width as above. The same geometry has been applied in the dynamical model used in this paper.

Table A2 contains the physical parameters of the sample sources derived from the model. The entries are:

Columns 2, 3 and 4: Age, equipartition energy density, and equipartition magnetic field strength with their estimated uncertainty, respectively – as described in Sect. 3.

Columns 5, 6 and 7: Logarithms of the jet power, initial density of the external medium at the core radius a_0 , and the cocoon pressure, respectively, derived from the model.

Column 8: Logarithms of the total source (cocoon) energy.

Column 9: Ratio between the total energy of twin jets and source energy.

Table 6: The sample

IAU name	Other name	z	$\lg P_{1.4}$ [$\text{WHz}^{-1}\text{sr}^{-1}$]	$D \pm \Delta D$ [kpc]	$\text{AR} \pm \Delta \text{AR}$	$\lg V_c \pm \Delta \lg V_c$ [kpc^3]	Ref. map	Spect. anal.
GIANTS								
0109+492	3C35	0.0670	24.53	1166±31	3.2±0.7	8.08±0.17	28	24
0136+396	B2	0.2107	25.21	1555±35	6.0±1.2	7.91±0.16	4	6
0313+683	WNB	0.0901	24.41	2005±34	4.2±0.5	8.55±0.10	28	23
0319-454	PKS	0.0633	24.70	2680±30	4.0±0.8	8.98±0.16	22	22
0437-244	MRC	0.84	26.15	1055±17	7.8±1.5	7.18±0.15	5	5
0813+758	WNB	0.2324	25.10	2340±80	5.0±0.5	8.60±0.08	25	24
0821+695	8C	0.538	25.28	2990±22	5.9±1.0	8.77±0.14	7	7
1003+351	3C236	0.0988	24.76	5650±75	9.4±1.7	9.20±0.14	15	16
1025-229	MRC	0.309	25.28	1064±17	5.2±0.7	7.54±0.11	5	5
1209+745	4C74.17	0.107	24.42	1090±13	2.4±0.5	8.25±0.16	2	24
1232+216	3C274.1	0.422	26.32	1024±15	7.4±1.6	7.19±0.17	8	1
1312+698	DA340	0.106	24.76	1085±12	4.4±0.9	7.71±0.16	28	24
1343+379		0.2267	24.42	3140±60	6.2±1.1	8.80±0.14	28,14	13
1349+647	3C292	0.71	27.02	1073±16	6.2±1.4	7.40±0.18	28	1
1358+305	B2	0.206	24.86	2670±60	3.6±0.8	9.06±0.17	19	19
1543+845	WNB	0.201	24.76	1950±25	7.6±1.4	8.00±0.15	28	24
1550+202	3C326	0.0895	25.02	2510±55	7.0±1.1	8.40±0.13	28	16
2043+749	4C74.26	0.104	24.86	1550±20	4.6±0.8	8.14±0.14	28	24
NORMAL								
0154+286	3C55	0.720	26.79	554±12	6.4±1.5	6.51±0.18	9	9
0229+341	3C68.1	1.238	27.26	414±10	4.4±1.0	6.46±0.18	9	9
0231+313	3C68.2	1.575	27.30	190±4	2.8±0.6	5.84±0.14	9	9
0404+428	3C103	0.330	26.32	564±12	6.7±1.0	6.50±0.12	8	1
0610+260	3C154	0.5804	26.84	376±10	2.9±0.8	6.70±0.21	9	9
0640+233	3C165	0.296	25.94	480±8	3.4±0.8	6.88±0.18	8	1
0642+214	3C166	0.246	26.66	187±15	3.1±0.6	5.73±0.15	8	1,29
0710+118	3C175	0.768	26.85	392±8	3.4±0.9	6.61±0.20	9	9
0828+324	B2	0.0507	24.36	396±14	3.2±0.4	6.68±0.10	12	6,20
0908+376	B2	0.1047	24.39	100±8	2.2±0.2	5.21±0.08	18	20
0958+290	3C234	0.1848	25.84	460±8	4.6±1.0	6.56±0.17	8	1
1008+467	3C239	1.786	27.51	94±3	2.6±0.7	4.98±0.21	10	10
1012+488	GB/GB2	0.385	26.17	694±13	2.2±0.3	7.73±0.11	12	29
1030+585	3C244.1	0.428	26.47	352±7	5.4±1.3	6.07±0.19	8	1
1056+432	3C247	0.749	26.85	105±4	3.1±0.7	4.98±0.18	10	10
1100+772	3C249.1	0.311	25.94	247±24	2.8±1.0	6.18±0.26	9	9
1111+408	3C254	0.734	26.85	107±4	2.5±0.3	5.19±0.10	10	10
1113+295	B2	0.0489	24.21	97±5	2.2±0.3	5.17±0.11	18	20
1140+223	3C263.1	0.824	27.31	45±5	2.2±0.4	4.17±0.14	10	10
1141+354	GB/GB2	1.781	26.68	97±3	3.0±0.4	4.90±0.11	11	29
1142+318	3C265	0.8108	27.19	644±16	5.4±1.7	6.86±0.24	9	1,9
1143+500	3C266	1.275	27.15	37±2	4.0±0.4	3.40±0.08	10	10
1147+130	3C267	1.144	27.17	327±8	4.4±0.7	6.15±0.13	9	9
1157+732	3C268.1	0.974	27.41	340±7	4.1±0.6	6.44±0.12	9	9
1206+439	3C268.4	1.400	27.37	87±4	2.8±0.3	4.82±0.09	10	10
1216+507	GB/GB2	0.1995	24.93	826±8	4.4±0.6	7.36±0.11	12	29
1218+339	3C270.1	1.519	27.48	104±12	2.6±0.5	5.12±0.15	10	10
1221+423	3C272	0.944	26.73	490±13	3.6±1.1	6.87±0.23	28	29
1241+166	3C275.1	0.557	26.56	130±15	2.0±0.4	5.63±0.16	10	10
1254+476	3C280	0.996	27.35	110±13	2.4±0.3	5.26±0.10	10	10
1308+277	3C284	0.2394	25.63	836±6	6.9±1.3	6.98±0.15	8	1

1420+198	3C300	0.270	26.00	516±6	3.0±1.2	7.08±0.29	8	1
1441+262	B2	0.0621	23.51	333±8	4.0±0.9	6.26±0.18	21	20
1522+546	3C319	0.192	25.56	390±15	3.2±0.7	6.66±0.17	8	1
1533+557	3C322	1.681	27.49	279±7	3.6±0.7	6.12±0.15	9	9
1609+660	3C330	0.549	26.93	458±8	6.4±1.2	6.27±0.15	9	9
1609+312	B2	0.0944	23.65	56±4	2.4±0.3	4.38±0.10	3	20
1615+324	3C332	0.1515	25.32	306±7	4.8±1.3	5.99±0.21	3	20
1618+177	3C334	0.555	26.45	430±15	2.8±0.4	6.90±0.12	9	9
1658+302	B2	0.0351	23.39	120±10	2.2±0.2	5.45±0.07	21	20
1723+510	3C356	1.079	26.96	643±13	7.9±1.0	6.52±0.10	9	9
1726+318	3C357	0.1664	25.43	395±10	3.0±0.6	6.73±0.16	21,3	20
1957+405	CygA	0.0564	27.25	185±3	3.8±0.5	5.54±0.11	9	9
2019+098	3C411	0.467	27.05	201±5	2.6±0.6	5.97±0.18	26	26
2104+763	3C427.1	0.572	26.75	173±5	2.9±0.7	5.68±0.19	9	9

References

- | | | |
|-----------------------------------|-------------------------------|---------------------------------|
| (1) Alexander & Leahy 1987 | (11) Machalski & Condon 1983 | (21) de Ruiter et al. 1986 |
| (2) van Breugel & Willis 1981 | (12) Machalski & Condon 1985 | (22) Saripalli et al. 1994 |
| (3) Fanti et al. 1986 | (13) Machalski & Jamrozy 2000 | (23) Schoenmakers et al. 1998 |
| (4) Hine 1979 | (14) Machalski et al. 2001 | (24) Schoenmakers et al. 2000 |
| (5) Ishwara-Chandra & Saikia 1999 | (15) Mack et al. 1997 | (25) Schoenmakers et al. 2001 |
| (6) Klein et al. 1995 | (16) Mack et al. 1998 | (26) Spangler & Pogge 1984 |
| (7) Lara et al. 2000 | (17) Myers & Spangler 1985 | (27) FIRST (Becker et al. 1996) |
| (8) Leahy & Williams 1984 | (18) Parma et al. 1986 | (28) NVSS (Condon et al. 1998) |
| (9) Leahy et al. 1989 | (19) Parma et al. 1996 | (29) this paper |
| (10) Liu et al. 1992 | (20) Parma et al. 2000 | |

Table 7: Age and physical parameters

Source	t [Myr]	$\lg u_{\text{eq}} \pm \Delta \lg u_{\text{eq}}$ [Jm ⁻³]	$B_{\text{eq}} \pm \Delta B_{\text{eq}}$ [nT]	$\lg Q_0$ [W]	$\lg \rho_0$ [kgm ⁻³]	$\lg p_c$ [Nm ⁻²]	$\lg U_{\text{eq}} \pm \Delta \lg U_{\text{eq}}$ [J]	$\frac{2Q_0 t}{U_{\text{eq}}}$
GIANTS								
0109+492	96±18	-13.74 ± 0.12	0.14±0.02	37.69	-24.03	-13.86	52.81±0.28	4.6±2.0
0136+396	89±17	-13.24 ± 0.17	0.25±0.05	38.29	-23.30	-13.36	53.14±0.31	8.0±4.2
0313+683	140±24	-14.11 ± 0.14	0.09±0.015	37.82	-23.87	-14.11	52.91±0.23	7.2±2.6
0319-454	180±40	-13.83 ± 0.13	0.13±0.02	38.07	-23.79	-14.15	53.62±0.28	3.2±1.3
0437-244	19±6	-12.37 ± 0.15	0.68±0.12	39.20	-23.37	-12.46	53.28±0.29	10.0±3.5
0813+758	84±4	-13.60 ± 0.15	0.17±0.03	38.47	-23.90	-13.79	53.47±0.22	5.3±2.5
0821+695	84±10	-13.37 ± 0.17	0.21±0.04	38.84	-23.68	-13.64	53.87±0.30	5.0±2.8
1003+351	127±18	-14.25 ± 0.14	0.08±0.013	38.62	-23.83	-14.34	53.42±0.27	12.8±6.1
1025-229	64±12	-12.82 ± 0.22	0.40±0.10	38.23	-23.25	-13.10	53.19±0.31	4.4±2.3
1209+745	110±20	-13.79 ± 0.13	0.13±0.02	37.60	-24.23	-13.99	52.93±0.28	5.3±1.5
1232+216	22±3	-12.29 ± 0.32	0.74±0.27	39.20	-23.20	-12.38	53.37±0.43	9.4±8.0
1312+698	55±5	-13.44 ± 0.14	0.19±0.03	37.95	-23.97	-13.56	52.74±0.29	5.7±3.2
1343+379	94±16	-14.20 ± 0.33	0.08±0.03	38.24	-24.16	-14.25	53.07±0.41	8.8±6.8
1349+647	16±4	-11.84 ± 0.17	1.25±0.25	39.79	-23.30	-12.07	54.03±0.33	5.8±3.0
1358+305	125±25	-13.95 ± 0.14	0.12±0.02	38.34	-24.12	-14.10	53.58±0.30	4.6±2.2
1543+845	130±21	-13.46 ± 0.23	0.19±0.05	38.03	-23.00	-13.61	53.01±0.35	8.6±5.6
1550+202	134±27	-13.63 ± 0.27	0.16±0.05	38.26	-23.21	-13.73	53.24±0.36	8.9±5.7
2043+749	64±11	-13.57 ± 0.10	0.17±0.02	38.14	-24.06	-13.74	53.04±0.23	5.1±1.9
NORMAL								
0154+286	13.0±1.7	-11.55 ± 0.16	1.74±0.32	39.43	-22.98	-11.72	53.43±0.32	8.2±5.0
0229+341	11.3±1.8	-11.31 ± 0.19	2.31±0.43	39.69	-22.91	-11.33	53.62±0.35	8.4±5.4
0231+313	4.6±0.3	-10.71 ± 0.16	4.58±0.85	39.64	-23.55	-11.03	53.60±0.29	3.2±1.9
0404+428	17.7±2.4	-11.91 ± 0.17	1.15±0.23	39.02	-22.96	-12.01	53.06±0.30	10.2±5.5
0610+260	45.2±3.8	-11.72 ± 0.18	1.43±0.30	39.00	-22.20	-11.54	53.45±0.36	10.2±7.6
0640+233	60±10	-12.34 ± 0.16	0.70±0.13	38.33	-22.66	-12.30	53.01±0.32	7.9±4.5
0642+214	14.0±5.0	-11.71 ± 0.22	1.44±0.37	38.87	-22.71	-11.23	52.56±0.34	17.9±7.9
0710+118	34.5±4.5	-11.54 ± 0.16	1.76±0.32	39.09	-22.31	-11.52	53.54±0.34	7.8±5.0
0828+324	59±9	-13.27 ± 0.18	0.24±0.05	37.20	-23.60	-13.24	51.88±0.27	7.8±3.6
0908+376	28.4±4.4	-12.33 ± 0.16	0.71±0.13	36.83	-23.36	-12.39	51.35±0.23	5.5±2.0
0958+290	22.0±4.0	-12.11 ± 0.15	0.92±0.16	38.53	-23.31	-12.32	52.92±0.30	5.7±2.9
1008+467	2.8±0.2	-10.28 ± 0.16	7.48±1.39	39.66	-23.21	-10.36	53.17±0.35	5.5±4.0
1012+488	38.5±5.5	-12.83 ± 0.13	0.40±0.06	38.81	-23.93	-12.80	53.37±0.23	6.7±2.6
1030+585	14.0±2.0	-11.56 ± 0.16	1.72±0.32	38.98	-22.84	-11.62	52.98±0.33	8.9±5.5
1056+432	3.2±0.3	-10.72 ± 0.14	4.55±0.71	39.18	-23.44	-10.81	52.73±0.31	5.7±3.5
1100+772	31.5±5.5	-11.92 ± 0.16	1.14±0.21	38.24	-22.87	-11.95	52.73±0.38	6.5±4.6
1111+408	3.1±0.2	-10.75 ± 0.15	4.40±0.76	39.20	-23.79	-10.97	52.91±0.24	3.8±1.9
1113+295	18.8±2.7	-12.42 ± 0.16	0.64±0.12	36.84	-23.84	-12.51	51.22±0.26	5.0±2.2
1140+223	1.7±0.6	-9.87 ± 0.11	12.0±1.50	39.38	-23.27	-10.02	52.77±0.24	4.4±1.0
1141+354	3.4±0.8	-10.69 ± 0.16	4.68±0.87	39.03	-23.44	-10.85	52.68±0.26	4.8±2.4
1142+318	22.0±5.0	-11.66 ± 0.16	1.54±0.29	39.64	-22.52	-11.57	53.67±0.37	13.0±8.1
1143+500	1.2±0.5	-9.67 ± 0.16	15.1±2.80	39.32	-22.65	-9.58	52.20±0.23	10.0±4.2
1147+130	12.5±3.6	-11.10 ± 0.14	2.93±0.48	39.51	-22.60	-11.16	53.52±0.26	7.7±2.4
1157+732	12.6±2.6	-11.17 ± 0.16	2.70±0.49 ²⁶	39.73	-22.73	-11.20	53.74±0.27	7.8±3.2
1206+439	3.0±0.3	-10.34 ± 0.12	7.00±1.00	39.52	-23.04	-10.32	52.95±0.20	7.1±2.6
1216+507	50±15	-13.11 ± 0.18	0.29±0.06	37.98	-23.73	-13.29	52.72±0.28	5.8±1.9
1218+339	3.9±1.1	-10.35 ± 0.17	6.90±1.35	39.60	-23.00	-10.41	53.24±0.30	5.7±2.4
1221+423	18.0±8.0	-11.94 ± 0.16	1.12±0.21	39.25	-23.26	-11.90	53.40±0.36	8.1±3.1
1241+166	4.2±0.4	-11.40 ± 0.16	2.07±0.38	39.01	-24.21	-11.44	52.70±0.30	5.5±3.3
1254+476	2.8±0.3	-10.68 ± 0.16	4.77±0.88	39.59	-23.64	-10.69	53.05±0.25	6.2±2.9
1308+277	60±9	-12.60 ± 0.18	0.52±0.11	38.37	-22.59	-12.63	52.85±0.31	12.6±7.2

1420+198	43±6	-12.27 ± 0.14	0.76±0.12	38.49	-23.22	-12.47	53.28±0.39	4.4±3.3
1441+262	77±13	-13.30 ± 0.19	0.23±0.05	36.49	-23.40	-13.46	51.43±0.35	5.6±3.5
1522+546	43±7	-12.33 ± 0.15	0.71±0.12	38.07	-23.13	-12.49	52.80±0.30	5.1±2.7
1533+557	7.3±0.6	-11.00 ± 0.16	3.28±0.60	39.82	-23.01	-10.99	53.59±0.30	7.9±4.7
1609+660	20.3±3.3	-11.39 ± 0.18	2.10±0.43	39.35	-22.19	-11.36	53.35±0.31	12.9±7.1
1609+312	11.5±2.5	-12.08 ± 0.14	0.95±0.15	36.42	-24.00	-12.39	50.77±0.23	3.3±1.0
1615+324	47±9	-12.24 ± 0.15	0.79±0.14	37.78	-22.40	-12.18	52.22±0.34	10.8±6.3
1618+177	31.6±3.7	-11.91 ± 0.15	1.15±0.20	38.83	-23.10	-12.07	53.46±0.26	4.7±2.2
1658+302	48.5±8.5	-13.05 ± 0.17	0.31±0.06	36.10	-23.67	-13.12	50.87±0.20	5.2±1.5
1723+510	20.0±2.6	-11.54 ± 0.18	1.76±0.36	39.55	-22.29	-11.53	53.45±0.27	16.0±7.7
1726+318	27.0±5.0	-12.48 ± 0.14	0.60±0.10	38.14	-23.76	-12.67	52.72±0.29	4.5±2.1
1957+405	12.6±3.0	-10.39 ± 0.15	6.60±1.18	39.39	-22.03	-10.61	53.62±0.25	4.7±1.6
2019+098	9.2±1.2	-11.14 ± 0.10	2.80±0.32	39.28	-23.20	-11.22	53.30±0.27	5.6±2.7
2104+763	7.7±0.6	-10.87 ± 0.14	3.80±0.63	39.06	-23.28	-11.25	53.28±0.31	2.9±1.9